 doi:10.20944/preprints202103.0107.v1

Thioredoxins *o*1 and *h*2 show different subcellular localizations and redox-active functions, but cooperatively affect NADPH redox poise and photosynthetic performance in fluctuating light

Liang-Yu Hou*, Martin Lehmann, Peter Geigenberger

Ludwig-Maximilians-University Munich, Department Biology I, 82152 Planegg-Martinsried, Germany

*For correspondence: Liang-Yu Hou (LiangYu.Hou@biologie.uni-muenchen.de)

Preprints (www.preprints.org) | NOT PEER-REVIEWED | Posted: 2 March 2021 doi:10.20944/preprints202103.0107.v1

Abstract

Arabidopsis contains eight different *h*-type thioredoxins (Trx) being distributed in different cell organelles. Although Trx *h*2 is deemed to be localized in mitochondria, its subcellular localization and function remains a matter of debate. Here, Trx *h*2 localization and function were investigated using cell fractionation studies and reverse genetics. Differential centrifugation and immunodetection showed the Trx *h*2 protein to be distributed to the microsomal fraction rather than to mitochondrial preparations. To analyze whether Trx *h*2 has different roles than mitochondrial Trxs, Arabidopsis mutants lacking Trx *h*2 were compared with mutants deficient in mitochondrial Trx *o*1 and double mutants with joint deficiencies in both Trxs. Under constant medium light, *trxh2* grew as the wild type, while *trxo1* and *trxo1h2* mutants showed impaired growth. This was accompanied by differences in the metabolite profiles. The *trxo1* and *trxo1h2* mutants clustered differently from the wild type during the night, revealing a decrease in ascorbate and glutathione redox states. In fluctuating light intensities, genotypic differences in growth rates were attenuated. Compared to the wild type, the fluctuating-light induced decrease in the NADPH/NADP ratio was diminished in the mutants, with the *trxo1h2* double mutant showing the strongest effect. This was accompanied by an increase in the photosynthetic efficiency of the *trxo1h2* mutant, specifically in the high light phases of fluctuating light. Conclusively, these results support the view that Trxs *o*1 and *h*2 are localized in different subcellular compartments, and have different effects on ascorbate and glutathione redox states and growth in medium light, but cooperatively affect NADP(H) redox state and photosynthetic efficiency in fluctuating light.

Keywords

Trx *o*1, Trx *h*2, metabolomics, ascorbate, glutathione, NAD(P)(H), photosynthetic performance, fluctuating light, *Arabidopsis thaliana*

Introduction

Reduction-oxidation reactions serve as fundamental components for the processes of bioenergetics and signal pathways. Proper operation of biosynthetic processes and signal transduction relies on the optimization of redox potential spans. This appears to be of importance for plants, since plants often encounter diverse environmental challenges. For example, light intensity in field changes very rapidly. Such fluctuation of light intensity leads to short-term imbalances in the redox state of

Preprints (www.preprints.org) | NOT PEER-REVIEWED | Posted: 2 March 2021 doi:10.20944/preprints202103.0107.v1

NADPH/$NADP^+$ and the energy state of adenylated nucleotides, and eventually results in the over-production of reactive oxygen species, which dramatically change the cellular redox poise [1,2]. Thus, plants develop several mechanisms to deal with such challenges.

Ascorbate (AsA) and glutathione (GSH) redox systems are known as powerful buffering mechanisms to balance cellular redox states [3]. Both AsA and GSH are able to metabolize hydrogen peroxide (H_2O_2). While both systems can work independently, they were also shown to function in an integrated manner [4]. In the AsA-GSH cycle, AsA serves as an electron donor for ascorbate peroxidase (APX) to detoxify H_2O_2. Then, AsA is converted into monodehydroascorbate (MDHA), which can be regenerated as AsA with the help of monodehydroascorbate reductase (MDHAR). Part of MDHA is subsequently converted into dehydroascorbate (DHA), which can also be reduced to AsA via the activity of dehydroascorbate reductase (DHAR) using glutathione as electron donors. This would generate oxidized glutathione disulfide (GSSG), which can be regenerated to GSH via the activity of glutathione reductase (GR) using NADPH as an electron donor. The reduced glutathione can then be used for the regeneration of AsA again or the detoxification of H_2O_2 [5]. The disruption of the AsA-GSH cycle greatly compromises plant stress tolerance as well as plant development [6–8]. Furthermore, there are growing reports indicating an interaction of AsA, GSH and thioredoxin (Trx) systems to maintain the cellular redox balance [9–13]. In this context, plastidial MDHAR was found to be redox-regulated by Trxs [14].

Thioredoxins are ubiquitous proteins in various organisms. Plants have the most elaborate Trx system, with respect to different reduction pathways and isoforms being involved in the redox regulation of widespread metabolic processes in different subcellular compartments [4]. In Arabidopsis, the 20 Trx isoforms are categorized into seven types: Trx *f*, *h*, *m*, *o*, *x*, *y* and *z* [15,16]. The *f*, *m*, *x*, *y* and *z*-type Trxs are plastidial proteins, and responsible for regulating redox balance and metabolic processes in chloroplasts, *e.g.*, enzyme activation of Calvin-Benson, carbon metabolism [17,18], the regulation of malate valve [19], meristem development, cyclic electron transport [20–22], the regulation of antioxidation systems [23–26], and plastidial gene expression [27].

The *o*-type Trxs comprise two isoforms, Trx *o*1 and *o*2. The Trx *o*1 protein is specifically localized in mitochondria, with the exception of pea (*Pisum sativum*), where this protein was found in both mitochondria and nuclei [28,29]. Work with

 doi:10.20944/preprints202103.0107.v1

Arabidopsis knock-out mutants and biochemical studies indicate diverse functions of Trx *o*1, including the regulation of stress responses and cell cycle progression, as well as activation of tricarboxylic-acid-cycle (TCA) enzymes and alternative oxidase (AOX) in respiratory processes of mitochondria [30–34], even though it is still under debate whether Trx *o*1 is involved in the redox regulation of AOX [35]. Furthermore, the Trx *o*1 protein has been suggested to be involved in the regulation of NAD(P)(H) redox state and the inhibition of mitochondrial glycine decarboxylase (GDC) L-protein, and thus be able to fine-tune photorespiratory processes in Arabidopsis [36].

The *h*-type Trxs are the largest Trx family, which contains eight isoforms. Many of *h*-type Trxs, including Trx *h*1, *h*3, *h*4, and *h*5, were found to be localized in cytosol, while Trx *h*7 and *h*8 were reported to be associated with ER-Golgi membrane compartments and Trx *h*9 was found to be localized at plasma membrane [28,37–39]. As the largest Trx family, the *h*-type Trxs were found to have diverse functions. In barley and wheat, Trx *h* is involved in the seed developmental processes [40,41]. In Arabidopsis, it has been reported that Trx *h*3 functioned as molecular chaperones to help plants overcome heat stress [42]. Trx *h*5 was strongly induced in response to pathogen infection and oxidative stresses [43,44]. Furthermore, Trx *h*9 plays a role in intercellular communication [37]. In contrast to the other *h*-type Trxs, Trx *h*2 was found to harbor regulatory functions in several metabolic pathways of mitochondria. The first report from Daloso et al. indicated Trx *h*2 to cooperate with Trx *o*1 to regulate TCA cycle enzyme activities [33]. With the analyses on *trxh2* Arabidopsis mutants, Trx *h*2 was found to be involved in photorespiratory processes via redox-regulating the activity of the mitochondrial GDC L-protein [45]. However, the subcellular localization of Trx *h*2 remained unclear. Using transient expression of GFP-fused Trx *h*2 protein in onion epidermal cells, Meng et al. suggested that the Trx *h*2 is localized in both cytosol and mitochondria [37], while Traverso et al. used the same approach to propose that this protein is also associated with the ER-Golgi membrane system [38].

The studies mentioned above suggest that Trx *h*2 is likely to share redundant functions with Trx *o*1 in mitochondria, while it remains unclear whether Trx *h*2 is indeed localized within this organelle. In the present work, we use cell fractionation studies as an additional technique to clarify the subcellular localization of the Trx *h*2 protein and confirmed its localization to the microsomal fraction, rather than to mitochondria. To further understand the role of Trx *h*2 in comparison to

Preprints (www.preprints.org) | NOT PEER-REVIEWED | Posted: 2 March 2021 doi:10.20944/preprints202103.0107.v1

mitochondrial Trx *o*1, we selected two Arabidopsis T-DNA insertion mutants (*trxo1* and *trxh2*) showing deficiencies of Trx *o*1 and Trx *h*2. Both lines have been comprehensively characterized in previous studies [33, 45] and therefore serve as representative T-DNA insertion mutants for the following analyses. Both lines were further crossed to generate a double mutant (*trxo1h2*) showing joint deficiencies of both Trxs. In experiments to directly compare these lines, the *trxo1* and *trxh2* single mutants showed different effects on the redox states of AsA and GSH as well as growth in medium light, while the *trxo1h2* double mutant showed additive effects on NADP(H) redox state and photosynthetic efficiency in fluctuating light. This indicates different roles of Trx *o*1 and *h*2 depending on the light conditions.

Results

The Trx *h*2 protein enriches in the microsomal fraction

Unlike the mitochondrial Trx *o*1, the subcellular localization of Trx *h*2 remains controversial. While previous studies used transient expression systems and reporter genes, here a cell fractionation approach was alternatively adopted to clarify this debating issue. Prior to the fractionation assay, the transcript and protein levels of Trx *h*2 in mutant lines were analyzed using real-time quantitative PCR and immunoblotting. There was no Trx *h*2 signal detectable in *trxh2* mutants, while the expression of Trx *h*2 in overexpression lines increased by 100 times wild-type level (Figure S1, A and B). This documents that both Trx *h*2 mutants and overexpression lines serve as proper material for the following assays.

Figure 1 shows the Trx *h*2 protein level in different subcellular fractions enriched in microsomes, cytosol and mitochondria, documented by immunoblots using calnexin (CNX), cytosolic fructose-1,6-bisphosphatase (cyt-FBPase) and alternative oxidase (AOX) as marker proteins, respectively. While fractionation assays were performed using plant material from the wild type, *trxh2* mutant and Trx *h*2 overexpression line (Trx $h2_{ox}$), the sensitivity of the antibody allowed the detection of the Trx *h*2 protein only in immunoblots from the Trx $h2_{ox}$ line, but not from the wild type. The Trx *h*2 protein was clearly present in the purified microsomal fraction of Trx $h2_{ox}$ plants, which was enriched in CNX, while no clear Trx *h*2 signals were detectable in purified cytosolic fractions (enriched in cyt-FBPase), and in purified mitochondria (enriched in AOX). These results support the view that the Trx *h*2 protein is confined to the microsomes, rather than to cytosol or mitochondria. However, more studies are necessary to increase the sensitivity of the

Preprints (www.preprints.org) | NOT PEER-REVIEWED | Posted: 2 March 2021 doi:10.20944/preprints202103.0107.v1

immuno-detection of Trx *h*2 to document its subcellular fractionation also in the wild type.

The *trxh2* and *trxo1* mutants show differential growth phenotypes when grown in different light conditions

Since Trx *h*2 showed a different subcellular localizations in comparison to Trx *o*1, we next investigated whether both proteins show differential functions. To do this, we analyzed *trxo1* [33] and *trxh2* [45] T-DNA insertion lines, which were shown to be representative lines in previous studies, together with a double mutant (*trxo1h2*) generated by crossing of these lines. In confirmation to previous studies on the *trxo1* [33] and *trxh2* [45] T-DNA insertion lines, the T-DNA inserted at the third exon of the Trx *h*2 gene in *trxh2*, while the T-DNA inserted at the first intron of the Trx *o*1 gene in *trxo1* (Figure 2A). Furthermore, the expression of Trx *h*2 gene in *trxh2* significantly decreased by 95% compared to the wild type, and the expression of Trx *o*1 gene in *trxo1* significantly decreased by 98% compared to the wild type. In the double mutant (*trxo1h2*), the expression of both Trx *h*2 and *o*1 was significantly decreased in comparison to the wild type (Figure 2B). This documents that these three different T-DNA insertion lines are null mutants and appropriate for the following applications.

To understand whether deficiency of Trx *h*2 and *o*1 affects plant growth, the growth phenotype of the mutant lines was analyzed. In addition to a standard growth condition with medium light intensity (ML), plants were also grown under fluctuating light intensity (FL), consisting of a loop of five-minute low light phase and one-minute high light phase, to mimic natural light conditions in the field. Under constant ML conditions, the growth of the *trxh2* mutant was comparable to the wild type, while *trxo1* single and *trxo1h2* double mutants showed retarded growth (Figure 3A). Surprisingly, this growth phenotype became subtle under FL conditions, in which all mutants grew like the wild type (Figure 3B). There is a general decrease in plant growth when FL is compared with constant ML conditions (Figure 3, A and B), with the decrease being less strongly expressed in *trxo1* and *trxo1h2* mutants. These data show that deficiency of Trx *o*1 leads to impaired plant growth under normal light conditions, but not in fluctuating light, while deficiency of Trx *h*2 has no effect on growth in any of the conditions.

Preprints (www.preprints.org) | NOT PEER-REVIEWED | Posted: 2 March 2021 doi:10.20944/preprints202103.0107.v1

Nocturnal metabolite levels of *trxh2*, *trxo1* and *trxo1h2* mutants cluster differently to the wild type

To further understand the differential effects of Trx *h*2 and *o*1 on plant growth, a GC-TOF-MS approach was performed to analyze metabolite profiles in the mutants under different light conditions. We first analyzed the data set using principle component analysis (PCA) to get a global pattern of metabolite changes. When nocturnal metabolism was investigated, the three mutants clustered differently to the wild type. The *trxo1* and *trxo1h2* mutants showed a similar cluster, while the *trxh2* single mutant was only overlapping partly with the *trxo1* mutant (Figure 4A). Interestingly, when metabolism was analyzed in the light, the PCA shows a similar cluster for the wild type and mutants. This holds true for the day phase of constant ML conditions (Figure 4B), as well as for the high light (HL) and low light (LL) phases of FL conditions (Figure 4, C and D). This indicates that Trx *h*2 and Trx *o*1 are both important for nocturnal metabolism, with partially overlapping functions

Indeed, in the end of night, the *trxh2* and *trxo1* single mutants and the *trxo1h2* double mutants showed a mild decrease in the levels of several soluble sugars, which were the cases for fructose (51-84% of wild-type level), glucoheptose (64-88% of wild-type level), raffinose (37-54% of wild-type level) and xylulose (81-88% of wild-type level), and amino acids, which were the case for arginine (76-84% of wild-type level), glutamine (71-88% of wild-type level), glycine (61-78% of wild-type level), methionine (85% of wild-type level), ornithine (63-80% of wild-type level), and serine (73-89% of wild-type level). Notably, in the mutant lines, the levels of 4-aminobutanoic acid (GABA) and phenylalanine were significantly increased when compared to the wild type (Figure 5, A and B, left panel; Table S1). In the mutant lines, there was also a clear decreasing pattern in the levels of many organic acids, including 2-piperidinecarboxylic acid (30-54% of wild-type level), adipic acid (56-71% of wild-type level), gluconic acid (68-88% of wild-type level), lactic acid (55-69% of wild-type level), ribonic acid (57-76% of wild-type level), pyruvic acid (71-82% of wild-type level), 2-oxoglutaric acid (69-82% of wild-type level) and succinic acid (67-81% of wild-type level; Figure 5C, left panel; Table S1). Surprisingly, joint deficiencies in Trx *h*2 and *o*1 had no additive effects on metabolite accumulation. However, these metabolite changes in the mutants versus wild type were not sustainable when metabolism in the light was analyzed (Figure 5, A, B and C, right panel; Table S1).

Under FL conditions, deficiency of Trx *h*2 an *o*1 had minor effects on the

Preprints (www.preprints.org) | NOT PEER-REVIEWED | Posted: 2 March 2021 doi:10.20944/preprints202103.0107.v1

accumulations of most sugars and sugar alcohols (Figure 5D). In the HL phases, the changes of most amino acids in the mutant lines were also very subtle, except for alanine (69-92% of wild-type level), glycine (75-91% of wild-type level) and proline (1.3-to-1.5 times wild-type level; Figure 5E, left panel, Table S2). However, in the LL phases, several amino acids showed significant changes in either the single or double mutants. This included glycine (1.3-to-1.5 times wild-type level), proline (1.2-to-1.4 times wild-type level), and O-acetyl-serine (68-76% of wild-type level; Figure 5E, right panel, Table S2). In the HL phases, some organic acids showed a decreasing tendency in the *trxo1* and *trxo1h2* mutants, which were the cases for galataric acid (80% of wild-type level), hexadecanoic acid (71-85% of wild-type level), ribonic acid (77% of wild-type level) and threonic acid (80% of wild-type level), while, in the LL phases, the changes were not sustainable (Figure 5F; Table S2). Taken together, the results indicate the significance of Trx *h*2 and *o*1 in nocturnal metabolism, while there were only minor effects in FL conditions.

Deficiencies in Trx *h*2 and *o*1 differentially affect the reduction states of ascorbate and glutathione

To understand whether Trx *h*2 and *o*1 are involved in the maintenance of cellular redox status, the reductive states of ascorbate (AsA)/dehydroascorbat (DHA) and reduced glutathione (GSH)/oxidized glutathione (GSSG) redox couples were analyzed. In the wild type, the total levels of AsA, DHA (Figure 6, A, B and C), GSH and GSSG (Figure 6, E, F and G) as well as the AsA and GSH reductive states (Figure 6, D and H) were higher in the different light conditions, compared to dark. When focusing on AsA system first, all three mutants showed a decrease in total AsA levels in the dark and HL phases, while *trxo1* single and *trxo1h2* double mutants also showed a decrease in ML conditions, compared to the wild type (Figure 6, A and C). In addition to this change, the AsA reduction state (calculated as the AsA/[AsA+DHA] ratio in %) in mutant lines except the *trxh2* single mutant was lower than the wild type under all analyzed conditions (Figure 6D). The decrease in AsA reduction state due to knockout of Trx *o*1 was more strongly expressed in the dark and ML than in FL conditions. Joint deficiencies of Trx *o*1 and *h*2 did not lead to stronger effects, compared to Trx *o*1 single deficiency.

Looking at the GSH system, all three mutants showed similar decreases in GSH levels (Figure 6E) and GSH redox states (Figure 6H; calculated as the GSH/[GSH+GSSG] ratio in %) and a increase in GSSG level (Figure 6F) under FL

Preprints (www.preprints.org) | NOT PEER-REVIEWED | Posted: 2 March 2021 doi:10.20944/preprints202103.0107.v1

conditions (HL and LL) compared to the wild type, while the similar patterns of three parameters in ML were observed in the *trxo1* single and *trxo1h2* double mutants, but not in the *trxh2* single mutant. In contrast to this change, GSH levels and GSH redox states were similar in all genotypes in the dark. The levels of total GSH pool in all three mutant lines were comparable to the wild type under all analyzed conditions (Figure 6G). These results indicate that both Trx *h*2 and *o*1 serve as positive regulators in maintaining the reductive state of the GSH system specifically in FL conditions, while Trx *o*1, but not Trx *h*2, regulates the reductive state of the AsA system under all analyzed conditions. This shows that Trxs *h*2 and *o*1 regulate the AsA and GSH redox systems in a different manner.

Deficiencies in Trx *h*2 and *o*1 affect the NADPH redox state in fluctuating light

The redox couples, NADPH/$NADP^+$ and NADH/NAD^+, are also important components for maintaining the cellular redox balance. They also serve as substrates for Trx reductases to regulate the redox state of Trxs. To understand whether deficiencies of Trxs *h*2 and *o*1 affect the redox balance of NAD(P)(H), the levels of NADPH, NADP, NADH and NAD were analyzed (Figure 7). In the wild type, the levels of NADPH (Figure 7A) and NADH (Figure 7D) as well as the NADPH/NADP (Figure 7C) and the NADH/NAD ratios (Figure 7F) were much higher in the light than in the dark, when plants were analyzed under constant ML conditions. This confirms previous studies showing a strong increase in the reduction states of the NADPH and NADH systems upon illumination under normal growth conditions [19,46]. Interestingly, the light-induced increase in the NADPH/NADP ratio was wiped out under FL intensities, yielding NADPH and NADP levels in HL and LL phases that were below those reached in night (Figure 7C). Also the light-induced increase in the NADH/NAD ratio was strongly attenuated in FL, compared to ML (Figure 7F).

In all three mutants, the levels of NADPH, NADP, NADH and NAD as well as the NADPH/NADP and NADH/NAD ratios were similar to the wild-type levels when plants were analyzed under ML conditions. Interestingly, there were increases in NADPH level (Figure 7A) and NADPH/NADP reduction state (Figure 7C) in mutants relative to the wild type, when plants were analyzed in FL intensities. The increase in these parameters was more markedly in LL compared to HL phases of FL conditions, and was more strongly expressed in the *trxo1* single and *trxo1h2* double mutants than in the *trxh2* single mutant. The *trxo1h2* double mutant reached the highest NADPH

Preprints (www.preprints.org) | NOT PEER-REVIEWED | Posted: 2 March 2021 doi:10.20944/preprints202103.0107.v1

level and NADPH/NADP ratio in the LL phases of FL, indicating that joint deficiencies of Trx *o*1 and *h*2 may lead to additive effects.

Taken together, illumination with a constant medium light intensity makes the redox couples, NADP(H) and NAD(H), maintain in reductive status, while illumination with frequently changed light intensities leads to a significant oxidation for the NADP(H) and NAD(H) redox couples. Furthermore, joint deficiencies in Trx *h*2 and *o*1 seems to attenuate the oxidation of NADPH induced by the fluctuation of light intensities, especially in the LL phases, while this deficiency has very minor effects on the redox state of NADH. These results indicate that both Trxs have negative effects on the levels and reduction states of NADPH in FL conditions.

Joint deficiencies in Trx *h*2 and *o*1 lead to enhanced photosynthetic efficiency in fluctuating light

The effects of Trxs *h*2 and *o*1 on NADPH reduction state in FL might be associated with changes in photosynthesis. Therefore, a pulse-amplitude-modulation (PAM) approach was used to analyze the photosynthetic performance of the mutants relative to the wild type. When plants grown in FL were analyzed, the quantum yield of photosystem II [Y(II)] decreased dramatically in HL versus LL phases of FL. This decrease in Y(II) was attenuated in the *trxo1h2* double mutant, showing a significantly higher Y(II) in the HL phases of FL, compared to the wild type or single mutants (Figure 8). In contrast to these changes in FL, the *trxo1h2* double mutant revealed only minor effects on Y(II) when plants were grown under constant ML conditions (Figure S2). Under steady state conditions of constant ML and dark, Y(II) levels of all mutants were similar to wild-type level. However, during dark-light transitions, the *trxo1h2* double mutant showed a faster increase in Y(II) kinetics (Figure S2), compared to the wild type or single mutants. These results indicate that Trxs *h*2 and *o*1 cooperatively affect photosynthetic performance under FL conditions and during rapid dark-light transitions, but have no sustainable effects on photosynthesis under steady state conditions in constant ML.

Discussion

Arabidopsis contains eight different *h*-type Trxs, which are distributed to different cell organelles. Although Trx *h*2 has been proposed to be localized specifically to mitochondria and to fulfill similar roles as mitochondrial Trx *o*1, its subcellular localization and function is still a matter of debate. In this work, we used a

Preprints (www.preprints.org) | NOT PEER-REVIEWED | Posted: 2 March 2021 doi:10.20944/preprints202103.0107.v1

cell fractionation approach to clarify the localization of Trx *h*2. To further understand the functions of Trx *h*2 and *o*1, we performed a series of physiological and biochemical analyses to compare representative trx*h*2 and trx*o*1 single mutants as well as their crossed double mutant in different light conditions. Our results show that Trx *h*2 is likely to be localized to the microsome, rather than to mitochondria. In constant light, Trx *h*2 and *o*1 harbor differential functions on plant growth, nocturnal metabolism and redox states of AsA and GSH, while, in fluctuating light, both types of Trxs jointly influence NADP(H) redox states and photosynthetic efficiency.

Thioredoxin *h*2 is most probably associated to ER/Golgi showing a different subcellular localization than Trx *o*1

The plant Trx *h* family consists of various isoforms, with Arabidopsis containing eight different *h*-type Trxs. Since the encoded proteins were found to have no obvious transit peptides, they were initially anticipated to be confined to the cytosol [39]. Interestingly, in further studies using transient expression systems and reporter genes, Trx *h*2 was proposed to localize to subcellular compartments other than the cytosol, but the results were not consistent. Studies by Gelhaye et al. and Meng et al. in poplar (*Populus trichocarpa*) and Arabidopsis proposed Trx *h*2 to reside in mitochondria [37,47], while Traverso et al. used similar studies in Arabidopsis to document that this protein is associated with the endoplasmic reticulum (ER)-Golgi membrane system [38]. To clarify the subcellular localization of Trx *h*2, we used a cell-fractionation study combined with immunoblot analyses in Arabidopsis. By analyzing Trx $h2_{ox}$ plants, we found the Trx *h*2 protein to enrich in microsomal fractions, while it was barely detectable in purified mitochondria or cytosolic fractions, providing direct biochemical evidence that Trx *h*2 is most likely confined to the endomembrane system, rather than to cytosol or mitochondria (Figure 1). However, immunodetection was not sensitive enough to allow the analysis of Trx *h*2 in the subcellular fractions of the wild type. More studies are necessary to improve the sensitivity of Trx *h*2 immunodetection. Our cell fractionation studies confirm the GFP reporter studies published by Traverso et al. [38]. Moreover, the Trx *h*2 protein was found to contain an N-terminal extension that harbors a myristoylated residue, which is known to target proteins to membranes [38]. When the N-terminal extension was removed, the modified Trx *h*2 was found to be relocalized to the cytosol, providing evidence that the N-myristoylation motif is responsible to induce the ER/Golgi localization of Trx *h*2 [38]. While N-myristoylation associates Trx *h*2 to Golgi/ER, cleavage of the fatty

Preprints (www.preprints.org) | NOT PEER-REVIEWED | Posted: 2 March 2021 doi:10.20944/preprints202103.0107.v1

acyl residue may relocate the protein to other subcellular compartments. It is however unresolved whether relocation of Trx *h*2 occurs in vivo and whether this is linked to its biological function or environmental/stress signals.

Thioredoxins *h*2 and *o*1 have different roles in regulating growth, ASA-GSH redox states and metabolite profiles in non-stressed conditions

To investigate whether the different subcellular localization relates to different functions of Trxs *h*2 and *o*1, we analyzed *trxh2* and *trxo1* single mutants together with a *trxo1h2* double mutant to allow a direct comparison of the different genotypes with respect to plant growth, cellular redox states, metabolite profiles and photosynthetic parameters under non-stressed ML conditions. Under these conditions, deficiency of Trx *o*1 led to a decrease in plant growth, while Trx *h*2 deficiency had no such effect (Figure 2). Interestingly, a joint deficiency of both Trxs did not lead to additive effects, indicating Trx *o*1 and *h2* to have different roles in growth regulation. The retardation of plant growth was not due to a decrease in photosynthetic efficiency, since the quantum yield of PS II was similar in all genotypes in ML (Figure S2).

The cellular redox status, which includes different redox systems, is important for metabolic regulation, antioxidant function and signaling, and ultimately determines plant growth and development. In non-stressed conditions, deficiencies in Trx *h*2 and *o*1 differentially affected the reduction states of the AsA/DHA and GSH/GSSG redox couples. Trx *o*1, but not Trx *h*2, deficiency led to a decrease in both AsA (Figure 6D) and GSH reduction states (Figure 6H). The *trxo1h2* double mutant showed similar changes as the *trxo1* single mutant with no substantial additive effects. In contrast to this, the NADPH/NADP and NADH/NAD redox couples in all mutant lines were similar to the wild type, with the exception of a nocturnal increase in NADPH/NADP redox state in the *trxh2* mutant. These results indicate that unlike Trx *h*2, Trx *o*1 is important to maintain the GSH and AsA redox states of the cell in non-stressed conditions. Since the AsA-GSH cycle mainly operates in mitochondria, but has not been documented in ER [48], results are in-line with the differential subcellular localization of Trxs *h*2 and *o*1, in Golgi/ER and mitochondria, respectively. This suggests that the different subcellular localization of both proteins is associated with different redox-active functions. It may also explain the differential effect of the two Trx proteins on plant growth.

Recently, with the proteomics analyses, several enzymes of the AsA-GSH cycle were found to be redox reactive and some of them were confirmed to be Trx targets

Preprints (www.preprints.org) | NOT PEER-REVIEWED | Posted: 2 March 2021 doi:10.20944/preprints202103.0107.v1

[14,49–52]. Indeed, from the in silico prediction, enzymes of AsA-GSH cycle harbor at least one putative redox-reactive Cys (Table S3), while whether the enzymes of AsA-GSH cycle are redox-regulated by Trx *h*2 and Trx *o*1 still requires further investigations.

Joint and single deficiencies of Trxs *h*2 and *o*1 also led to marked changes in nocturnal metabolite profiles, while there were no substantial changes in the profiles monitored in the light phase (Figure 4; Figure 5). The PCA of nocturnal metabolite profiles showed that all three mutant lines clustered differently from the wild type (Figure 4A). However, *trxh2* was only partly overlapping with these mutants and clusters more closely to the wild type, even though *trxo1* and *trxo1h2* clustered together. Thus, Trxs *h*2 and *o*1 partially affect global metabolite profiles in different manners, but it will not lead to additive effects when both Trxs are deficient. This further indicates that Trx *h*2 and *o*1 only share partially overlapping functions. The metabolic pathways where deficiencies of Trxs *h*2 and *o*1 led to similar pattern in metabolite profiles are as follows.

First, the levels of TCA cycle intermediates were generally decreased in the mutants (Figure 5; Table S1). The results are in line with previous studies proposed that Trx *o*1 and *h*2 are involved in the enzyme activation of TCA cycle [33]. Secondly, in addition to the changes in TCA cycle metabolites, there was an extremely strong increase of GABA in all mutant lines (Figure 5B; Table S1). Because the level of GABA precursor, Glu, was not changed in the mutants, it is likely that the accumulation of GABA is due to the degradation of polyamine, such as putrescine and spermidine [53,54]. The level of putrescine was actually decreased in all mutants (Table S1). Moreover, the over accumulation of GABA indicates that the carbon flow of TCA cycle in the mutants was compromised, so plants were alternatively elevating carbon flux through the GABA shunt to bypass the compromised activity of TCA cycle enzymes [55]. Thirdly, down-regulating the metabolism of organic acids is very likely to compromise the metabolism of amino acids, since organic acids serve as the major source of carbon skeleton for biosynthesis of amino acids. As expected, the levels of many amino acids, including Gly, Ser, Gln, Met, Orn and Arg, were decreased in the mutants (Figure 5B; Table S1). Notably, the concomitant decreases of Orn and Arg indicate a possible perturbation of Arg biosynthesis pathway [56]. In comparison to other amino acids, Arg harbors a high N:C ratio and acts as important nitrogen storage compound. It is also a precursor for the biosynthesis of polyamines and other nitrogen containing compounds [57,58]. Thus, perturbation in Arg

Preprints (www.preprints.org) | NOT PEER-REVIEWED | Posted: 2 March 2021 doi:10.20944/preprints202103.0107.v1

biosynthesis might subsequently lead to negative effects on nitrogen metabolism. However, it is unlikely that Trx *h*2 and *o*1 are able to regulate the enzymes of Arg biosynthesis pathway directly [56], since most of them reside in plastids. Thus, the down-regulation in Arg synthesis might be due to the shortage of organic acids. Fourthly, during the day, the levels of photorespiratory intermediates, such as Gly, Ser and glycerate, in the mutant lines were comparable to the wild type (Figure 5B; Table S1). However, it should be noted that plants grown in normal air where the contributions of Trx *h*2 and *o*1 to photorespiration are expected to be of minor importance. Indeed, the *trxh2* and *trxo1* single mutants showed comparable carbon assimilation rates to the wild type when grown under normal air conditions [36,45].

Interestingly, joint deficiencies of Trx *h*2 and *o*1 had no substantial additive effects on the accumulation of most metabolites, which makes it difficult to assess how both proteins cooperate in metabolic regulation. Since Trxs *h*2 and *o*1 are located in ER/Golgi and mitochondria, respectively, communication between the two different organells is required. Recently, genetically encoded reporters were used to document that there is a physical membrane contact between ER and mitochondria [59]. In addition to this, a physiological connection between ER and mitochondria is associated to ROS levels and the regulation of photorespiration [60]. More work will be required to analyze ER-mitochondria interactions in the regulation of plant metabolism in more detail.

Thioredoxin *h*2 and *o*1 cooperatively affect photosynthetic efficiency in fluctuating light

Plants have to manage strong light fluctuations in the field. Rapid alterations in light intensity strongly affect the availability of light energy for photosynthetic electron transport and carbon fixation and require efficient acclimation mechanisms to maintain photosynthetic efficiency and plant growth [1,2]. It has been found that light-dependent chloroplast Trxs play a crucial role in dynamic acclimation of photosynthesis in fluctuating light [19]. Our results show that this extends also to NADPH-dependent extra-plastidial Trxs. Intriguingly, the *trxo1h2* double mutant revealed a higher photosynthetic efficiency than the wild type and single mutants under fluctuating light, especially in the HL phases (Figure 8; Figure S3). This indicates that the extra-chloroplastidic Trxs *h*2 and *o*1 act in a cooperative manner to dampen acclimation processes in fluctuating light.

 doi:10.20944/preprints202103.0107.v1

Acclimation processes in fluctuating light were proposed to be important to avoid imbalances in NADPH/NADP redox states. However, studies are largely lacking to test this notion. Our results confirm the vulnerability of the NADPH/NADP redox state in fluctuating light conditions. In the wild type, there is a strong decline in the NADPH/NADP redox state in fluctuating light, compared to constant ML, which is quite dramatic since it drops down below nocturnal levels (Figure 7C). Interestingly, in the *trxo1h2* double mutant, the FL-dependent decrease in the NADPH/NADP ratio was attenuated, specifically in the LL phase of FL (Figure 7C), which is in-line with its improved photosynthetic efficiency under these conditions. This indicates that the cooperative effect of extra-plastidial Trxs *h*2 and *o*1 on FL-dependent acclimation processes is linked to NADPH redox homeostasis. The underlying mechanisms, however, remain unresolved. At the moment, it is unclear how Trxs *h*2 and *o*1, which are associated to Golgi/ER and mitochondria, respectively, can affect FL-acclimation processes that are known to reside in the chloroplast [61]. The cellular NADPH homeostasis is known to be mediated by inter-organellar malate/oxaloacetate shuttles involving the activities of different malate dehydrogenase (MDH) proteins distributed to chloroplasts, mitochondria, peroxisomes and cytoplasm [62]. Proteomics studies suggested that MDH proteins might act as targets of *h*-type Trxs [50,51]. Moreover, the activity of NAD-dependent MDH seems to be regulated by Trx *o*1 [33]. Taken together, it is likely that Trx *h*2 and *o*1 might cooperatively modulate the activity of MDH isoforms, and thus affect the cellular redox balance of NADPH and finally photosynthetic efficiency in FL.

Acclimation in fluctuating light has also been proposed to involve a stimulation of photorespiratory processes [63–65], providing an alternative explanation for the cooperative role of Trxs *h*2 and *o*1 in this context. Deficiencies of Trx *h*2 and *o*1 have been found to enhance the activity of glycine decarboxylation in mitochondria to facilitate photorespiratory carbon flow [36,45]. Enhancing photorespiratory carbon flow is proposed to promote photosynthesis [66,67]. It is quite likely that this mechanism is specifically important in FL conditions, which require elevated photorespiratory capacities [63–65]. Indeed, single and joint deficiencies of Trx *h*2 and *o*1 affected Gly level in FL conditions, leading to an increase in the LL phase, while there was a decrease in the HL phase of FL (Figure 5E). This suggests that Trxs *h*2 and *o*1 proteins are operating as negative effectors of FL acclimation, since they negatively regulate photorespiratory capacity under these conditions. Further investigations are required to confirm the two hypotheses mentioned above and to

 doi:10.20944/preprints202103.0107.v1

decipher the underlying regulatory mechanisms. The physiological connections between ER, mitochondria and chloroplasts may also be facilitated by direct membrane contact sites [59].

Conclusion

This study provides biochemical evidence that Trx *h*2 proteins are most likely associated to microsomes rather than to mitochondria, documenting a different localization in comparison to Trx *o*1. The different subcellular localization of both proteins is associated with different redox-active functions, with Trx *o*1, but not Trx *h*2, being important to maintain the AsA and GSH redox states and plant growth in non-stressed conditions. In contrast to this, there is a cooperative role of both Trxs *o*1 and *h*2 in regulating NADPH redox balance and photosynthetic performance in fluctuating light environments. This suggests a possible physiological interaction of both proteins between ER/Golgi and mitochondria, which extends to photosynthetic acclimation in the chloroplast.

Preprints (www.preprints.org) | NOT PEER-REVIEWED | Posted: 2 March 2021 doi:10.20944/preprints202103.0107.v1

Materials and Methods

Plant material and growth conditions

The Arabidopsis wild type, Columbia-0 (Col-0), two representative T-DNA insertion mutants, *trxh2* (SALK-079516) [45] and *trxo1* (SALK-042792) [33], and one crossed double mutant, *trxo1h2*, were used for this study. Both *trxh2* (SALK-079516) and *trxo1* (SALK-042792) have been comprehensively characterized in previous studies [33, 45] and therefore serve as representative T-DNA insertion mutants. Both lines were crossed to generate a double mutant (*trxo1h2*) showing joint deficiencies of both Trxs. All plants were grown under constant medium light (ML) or fluctuating light (FL). The light intensity of ML was set as 150 µmol m^{-2} s^{-1} with a 16-h-light/8-h-dark regime. Plants were grown under ML for three weeks, and the entire rosette leaves were harvested at the end of night (EN) and end of day (ED), respectively. The setup of FL contained loops of 5 min low light (LL, 50 µmol m^{-2} s^{-1}) and 1 min high light (HL, 500 µmol m^{-2} s^{-1}) with a 12-h-light/12-h-dark regime. Plants were grown under FL for four weeks, and the entire rosette leaves were harvested during the LL and HL phases, respectively, in the middle of day. The growth temperature was maintained in 22°C for both conditions.

Cell fractionation

Cytosolic fraction isolation

The cytosolic fraction isolation was performed as described before [68]. In brief, 2 g of 2-week-old seedlings was homogenized in the homogenization buffer (50 mM Tris-HCl, pH7.5; 250 mM sucrose; 5% glycerol; 10 mM EDTA; 0.5% [w/v] PVP-10; 3 mM DTT; 1 mM PMSF) on ice, and the cell debris were removed using miracloth followed by centrifugation for 10 min at 8000 x *g* in 4°C. The supernatant was transferred into a new tube and centrifuged for 10 min at 16000 x *g* in 4°C. The pellet was discarded, and the supernatant was centrifuged for 30 min at 100000 x *g* in 4°C. Afterward, the supernatant was also kept on ice for latter use.

Mitochondrion isolation

The mitochondrion isolation was performed as described before [69] with modifications. In brief, 30 g of 2-week-old seedlings was homogenized in 250 mL of extraction medium (300 mM sucrose 1.5 mM EDTA; 15 mM MOPS; 0.4% [w/v] fatty acid-free BSA; 0.6% [w/v] PVP-K30; 100 mM AsA; 10 mM DTT; pH 7.4) on ice. The leaf debris were removed using miracloth followed by centrifugation for 5

Preprints (www.preprints.org) | NOT PEER-REVIEWED | Posted: 2 March 2021 doi:10.20944/preprints202103.0107.v1

min at 1500 x *g* in 4°C. The pellet was kept on ice in the dark for latter chloroplast isolation. The supernatant was transferred into a new tube and centrifuged for 20 min at 16000 x *g* in 4°C. The pellet was carefully re-suspended in 1 mL of washing buffer I (300 mM sucrose; 10 mM TES; 0.1% [w/v] fatty acid-free BSA; pH 7.5) and mixed with 250 mL of washing buffer I followed by centrifugation for 5 min at 1500 x *g* in 4°C. The supernatant was transferred into another tube and centrifuged for 20 min at 16000 x *g* in 4°C. The pellet was carefully re-suspended in 1 mL of washing buffer and kept on ice in the dark for latter use. The separation buffer was made of heavy gradient solution (7 mL of 2-times strength washing medium I; 3.9 mL of Percoll; 3.1 mL of 20% [w/v] PVP-K30) and light gradient solution (7 mL of 2-times strength washing medium I; 3.9 mL of Percoll; 3.1 mL of double distilled water) using a gradient maker. Re-suspended pellet was carefully transferred onto the top of separation buffer followed by centrifugation with slow acceleration and disengaged brake for 40 min at 27000 x *g* in 4°C. The purified mitochondria were transferred into a new tube and washed with 40 mL of washing medium II (300 mM sucrose; 10 mM TES; pH 7.5) followed by centrifugation for 15 min at 16000 x *g* in 4°C. The mitochondrial pellet was kept on ice for latter use.

Microsome isolation

The microsome isolation was performed by using the kit (Minute™ Plant Microsomal Membrane Extraction Kit; Invent Biotechnologies). In brief, 200 mg of fresh plant leaves were homogenized in 300 µL of cold buffer A, and then transferred into a filter cartridge followed by centrifugation for 20 min at 14000 x *g* in 4°C. The supernatant was removed and the pellet was re-suspended in 300 µL of cold buffer B followed by centrifugation for 10 min at 11000 x *g* in 4°C. The supernatant was then transferred into a 2 mL microtube with the supplement of 1 mL of one-time strength PBS. The mixture was centrifuged for 30 min at 14000 x *g* in 4°C. The supernatant was removed and the pellet was kept on ice for latter use.

Protein extraction and immunoblotting analyses

Above samples were mixed with one-time strength Laemmli buffer [70] and incubated in 85°C for 15 min followed by centrifugation for 5 min at 20000 x *g* in 25°C. Ten microliter of supernatant was applied into a 4%-to-20% SDS acrylamide gradient gel for electrophoresis followed by transferred onto a 0.45 µm PVDF membrane for immunoblotting analyses. The antibody dilution factors were listed

Preprints (www.preprints.org) | NOT PEER-REVIEWED | Posted: 2 March 2021 doi:10.20944/preprints202103.0107.v1

below: thioredoxin *h*2 (Trx *h*2), 1:250; alternative oxidase (AOX), 1:1000; cytosolic fructose 1,6-bisphosphatase (cFBPase), 1:2500; calnexin (CNX): 1:5000. The Trx *h*2 antibody was produced by ThermoFisher Scientifc, and the others were purchased from Agrisera.

Molecular characterization

Total RNA extraction

Fifty milligram of ground leave sample was suspended in 500 µL of RNAzol reagent (Sigma), and then mixed with 100 µL of ice-cold chloroform followed by the centrifugation for ten min at 20,000 x *g* in 4°C. The upper aqueous phase was transferred into a new tube followed by the addition of 300 µL of isopropanol and the centrifugation for ten min at 20,000 x *g* in 4°C. The precipitated RNA pellet was suspended in 200 µL of nuclease-free water followed by the addition of 200 µL of PCI reagent (phenol/chloroform/isoamylalcohol, 25:24:1 [v/v/v]). The mixture was centrifuged for ten min at 20,000 x *g* in 4°C, and the upper phase was transferred into a new tube followed by the addition of 20 µL of 3 M sodium acetate and 500 µL of absolute ethanol. The whole mixture was centrifuged for ten min at 20,000 x *g* in 4°C. The precipitated RNA pellet was washed with 70% (v/v) ethanol and dehydrated in the hood. Afterward, the pellet was dissolved in 50 µL of nuclease-free water. The concentration was determined by a spectrophotometer (NanoFrop™ 2000, ThermoFisher Scientific).

Reverse transcription reaction

Five hundred nanogram of total RNA was incubated with the mixture containing 2 µL of 5-times reaction buffer and 0.5 µL of iScript reverse transcriptase (Biorad), and supplied with sufficient nuclease-free water to make up 10 µL in total volume. The reactions were performed in the thermo cycler (C1000 Touch™ Thermo Cycler, Biorad) with the program: 25°C for 10 min, 42°C for 30 min, and 85°C for 5 min. The cDNA sample was diluted for 10 times with nuclease-free water prior to the real-time quantitative PCR.

Real-time quantitative PCR

Five microliter of cDNA sample was incubated with the reaction mixture containing 10 µL of 2-times SYBG reagent (Biorad), 0.5 µL of 10 µM forward primer, 0.5 µL of 10 µM reverse primer and 4 µL of nuclease-free water. The reaction was

Preprints (www.preprints.org) | NOT PEER-REVIEWED | Posted: 2 March 2021 doi:10.20944/preprints202103.0107.v1

carried out in the thermo cycler (iQ5 Multicolor Real-Time PCR Detection System, Biorad) with the program: 95°C for 1 min, and 40 cycles, each containing 95°C for 30 sec, 60°C for 30 sec and 72°C for 30 sec. For building up the melting curve of primers, the temperature stared at 55°C and gradually elevated to 95°C in 0.5°C increments. The gene expression was quantified followed the $2^{-\Delta\Delta Ct}$ method [71,72]. The primer sequences were listed in the following: TRXh2-F (5'-catgccatggctgataagttcaatg-3'), TRXh2-R (5'-tcaagttcgtccttttttggcacc-3'), TRXo1-F (5'-gcctggtgtggaccatgcag-3'), TRXo1-R (5'-cagtgttggcacagccgtgat-3'), EF1α-F (5'-tgagcacgctcttcttgctttca-3') and EF1α-R (5'-ggtggtggcatccatcttgttaca-3').

Metabolite profiling

Total metabolite extraction

Fifty milligram of ground leave material was suspended in the extraction buffer containing 340 µL of ice-cold methanol, 10 µL of ribitol solution (0.2 mg mL^{-1}) and 10 µL of ^{13}C-sorbitol (0.2 mg mL^{-1}), followed by the incubation on ice for 30 min. The extract was further mixed with 200 µL of chloroform and 400 µL of water followed by the centrifugation for 15 min at 25,000 x *g* in 4°C. Fifty microliter of upper aqueous phase was transferred into a glass vial, and dehydrated using a vacuum at ambient temperature.

Gas chromatography coupled time-of-flight mass spectrometry

The detection of metabolite followed the method published before [73–75]. The details of sample preparation and condition were also described in the previous publication [76]. The results were analyzed using ChromaTOF 4.5 and TagFinder 4.5 softwares [77].

Measurement of metabolites

Ascorbate and dehydroascorbate

The assay followed the protocol described before [78]. In brief, 20 mg of pulverized leaf material was suspended in 200 µL of HCl solution (0.2 M) with vortex for 4 min followed by centrifugation for 10 min at 16000 x *g* in 4°C. Two hundred microliter of supernatant was transferred to a new microtube followed by the addition of 20 µL of NaH_2PO_4 solution (0.2 M, pH 5.6) and sufficient amount of NaOH solution (0.2 M) to make the pH value stay between five and six. The extract was kept on ice until further use.

Preprints (www.preprints.org) | NOT PEER-REVIEWED | Posted: 2 March 2021 doi:10.20944/preprints202103.0107.v1

For the measurement of AsA, 20 µL of extract was mixed with 100 µL of NaH_2PO_4 solution (0.2 M, pH 5.6) as well as 75 µL of double distilled water, and the opacity density at 265 nm was recorded every minute using the spectrophotometer (FilterMax F5, Molecular Device). When the reaction was stable, 2 µL of AsA oxidase (50 U mL^{-1}) was applied into the mixture to initiate the reaction. The decrease of optical density at 265 nm represents the AsA amount.

For the measurement of total ascorbate, 30 µL of extract was pre-incubated with 3 µL of DTT (25 mM) and 42 µL of NaH_2PO_4 solution (0.12 M) for 30 min in 25°C. Twenty microliter of this mixture was used for the measurement as above. Subtracting the reduced AsA amount from total ascorbate yields the amount of DHA.

The pure AsA and DHA were used to prepare standard solution for generating the calibration curve.

Glutathione and glutathione disulfide

The extraction followed the same approach mentioned above. For the measurement of total GSH, 10 µL of extract was mixed with 130 µL of reaction buffer (154 mM NaH_2PO_4, pH 7.5; 15.4 mM EDTA; 0.77 mM NADPH; 0.92 mM DTNB; 0.2 U GSH reductase) and 60 µL of double distilled water. The optical density at 412 nm was recorded every 30 sec using the spectrophotometer (FilterMax F5, Molecular Device). The reaction slope was used for the following calculation.

For the measurement of GSSG, 120 µL of extract was pre-incubated with 2 µL of 2-vinylpyrine for 30 min in 25°C to complex free GSH followed by centrifugation for 5 min at 20000 x *g* in 25°C. Ten microliter of the supernatant was used for the measurement as above. Subtracting double amounts of GSSG from total glutathione yields the amount of reduced GSH.

The pure GSH and GSSG were used to prepare standard solution for generating the calibration curve.

Pyridine nucleotides

The assay followed the protocol described before [79]. The details of sample preparation and detection were performed as described in the previous publication [76]

Preprints (www.preprints.org) | NOT PEER-REVIEWED | Posted: 2 March 2021 doi:10.20944/preprints202103.0107.v1

Pulse-Amplitude-Modulation measurement

Constant medium light treatment

Three-week-old plants grown under medium light were place in the dark for 30 min prior to the measurement, and shifted into the image PAM instrument (MAXI version, WALZ). The program was set as below: 20 min for constant medium light (150 μmol m^{-2} s^{-1}) followed by 10 min for the dark. The florescence signals were recorded every 30 sec.

Fluctuating light treatment

Four-week-old plants grown under fluctuating light were place in the dark for 30 min prior to the measurement, and shifted into the image PAM instrument. The program was set as below: 4 cycles of fluctuating light containing loops of 5 min low light (50 μmol m^{-2} s^{-1}) and 1 min high light (500 μmol m^{-2} s^{-1}), and 5 min for the dark. The florescence signals were recorded every 30 sec.

Calculation

The yield of photosystem II, Y(II) was calculated via the formula listed below: $Y(II) = (F_m' - F) / F_m'$. F, fluorescence yield measured briefly before application of a saturation pulse; F'_m, maximal fluorescence yield of illuminated sample with all PSII centers closed

Statistical analysis

The Graphpad Prism (version 8.0) was used to generate figures and carry out statistical analyses. The differences between genotypes were assayed via ANOVA followed by Dunnett's post-hoc test unless otherwise described. The R program was used to generate heatmap of metabolite profile and perform principle component analysis.

Accession numbers

Sequence data of this article is availabel from GeneBank/EMBL database. *Arabidopsis thaliana* Trx *h*2: At5g39950, Trx *o*1: At2g35010.

Data availability statement

All data has been included in this manuscript and the supplemental information.

Preprints (www.preprints.org) | NOT PEER-REVIEWED | Posted: 2 March 2021 doi:10.20944/preprints202103.0107.v1

Supplemental information

Figure S1. Molecular characterization of Trx *h*2 knock-out mutant (*trxh2*) and over expression line (Trx $h2_{ox}$).

Figure S2. The quantum yield of photosystem II [Y(II)] in the wild type (Col-0) and the mutant lines (*trxh2*, *trxo1* and *trxo1h2*) in medium light.

Table S1. Fold changes in metabolite profiles in Arabidopsis leaves of the wild type (Col-0) and thioredoxin mutant lines (*trxh2*, *trxo1* and *trxo1h2*) grown in non-stressed medium-light conditions.

Table S2. Fold changes in metabolite profiles in Arabidopsis leaves of the wild type (Col-0) and thioredoxin mutant lines (*trxh2*, *trxo1* and *trxo1h2*) grown in fluctuating light conditions.

Table S3 Prediction of conserved cysteine in enzymes of AsA-GSH cycle.

Figure legends

Figure 1. The enrichment of Trx *h*2 protein in different subcellular fractions. The wild-type plants (Col-0), knock out mutant (*trxh2*) and over expression line (Trx $h2_{ox}$) were grown under medium light condition for two weeks, and harvested for sample preparation. The detection of the TRXH2 protein and other subcellular protein markers was performed via immunoblot analysis. Calnexin (CNX) served as microsomal marker; cytosolic fructose-1,6-bisphosphatase (cyt-FBPase) served as cytosolic marker; alternative oxidase (AOX) served as mitochondrial marker.

Figure 2. Molecular characterization of *trxh2*, *trxo1* and *trxo1h2*. A, The scheme of T-DNA insertion sites in *trxh2* and *trxo1* mutants. B, The transcript levels of Trx *h*2 and Trx *o*1 in mutant lines compared to the wild type (Col-0). Mean values and standard errors derived from 6 biological replicates. The statistical analyses were performed by using ANOVA and the Dunnett's test (*$P < 0.05$, in comparison to the wild type).

Figure 3. Growth phenotype of the wild type (Col-0) and mutant lines (*trxh2*, *trxo1* and *trxo1h2*) grown under medium (ML) or fluctuating (FL) light conditions. A, Visible phenotype of rosette leaves. B, The box plot of leaf size. Mean values derived from 10 to 14 plants. The statistical analyses were performed by using ANOVA and the Dunnett's test (*$P < 0.05$, in comparison to the wild type). Scale bar = 2 cm.

Preprints (www.preprints.org) | NOT PEER-REVIEWED | Posted: 2 March 2021 doi:10.20944/preprints202103.0107.v1

Figure 4. The principle component analysis on metabolite profile of the wild type (Col-0) and the mutant lines (*trxh2*, *trxo1* and *trxo1h2*). Arabidopsis plants grown under medium light condition were harvested at the end of night (A) and the end of day (B), respectively. Arabidopsis grown under fluctuating light condition were harvested at the high light phase (C) and low light phase (D), respectively. The samples were used for metabolite profiling via GC-TOF-MS, and the results were used for principle component analysis by using R software. Dim 1: 1st principle component; Dim 2: 2nd principle component.

Figure 5. Metabolite profile of the wild type (Col-0) and the mutant lines (*trxh2*, *trxo1* and *trxo1h2*). Arabidopsis plants grown under medium light condition (A, B and C) were harvested at the end of night (EN) and the end of day (ED), respectively. Arabidopsis grown under fluctuating light condition (D, E and F) were harvested at the high light phase (HL) and low light phase (LL), respectively. The samples were used for metabolite profiling via GC-TOF-MS. A and D, Sugars and sugar alcohols. B and E, Amino acids. C and F, Organic acids and TCA cycle intermediates. Results are normalized to Col-0 with $\log_2$ transformation and visualized as a heatmap with hierarchical clustering done by R software. Data are taken from Table S1 and S2.

Figure 6. The redox couples of ascorbate (AsA) and glutathione (GSH) in the wild type (Col-0) and the mutant lines (*trxh2*, *trxo1* and *trxo1h2*). Arabidopsis plants grown under medium light condition were harvested at the end of night (EN) and the end of day (ED), respectively. Arabidopsis grown under fluctuating light condition were harvested at the high light phase (HL) and low light phase (LL), respectively. A, The level of ascorbate. B, The level of dehydroascorbate (DHA). C, The level of total AsA. D, The reduction state of AsA. E, The level of reduced GSH. F, The level of oxidized glutathione (GSSG). G, The level of total GSH. H, The reduction state of GSH. Mean values and standard errors derived from 6 biological replicates. The statistical analyses were performed by using ANOVA and the Dunnett's test (*P < 0.05, in comparison to the wild type).

Figure 7. The redox couples of NADP(H) and NAD(H) in the wild type (Col-0) and the mutant lines (*trxh2*, *trxo1* and *trxo1h2*). Arabidopsis plants grown under medium light condition were harvested at the end of night (EN) and the end of day (ED), respectively. Arabidopsis grown under fluctuating light condition were harvested at the high light phase (HL) and low light phase (LL), respectively. A, The level of NADPH. B, The level of NADP. C, The NADPH-to-NADP ratio. D, The level of NADH. E, The level of NAD. F, The NADH-to-NAD ratio. Mean values and

Preprints (www.preprints.org) | NOT PEER-REVIEWED | Posted: 2 March 2021 doi:10.20944/preprints202103.0107.v1

standard errors derived from 6 biological replicates. The statistical analyses were performed by using ANOVA and the Dunnett's test (*P < 0.05, in comparison to the wild type).

Figure 8. The quantum yield of photosystem II [Y(II)] in the wild type (Col-0) and the mutant lines (*trxh2*, *trxo1* and *trxo1h2*) in fluctuating light. Arabidopsis plants were grown in a fluctuating light environment for four weeks. Chlorophyll florescence kinetics during the alternating periods of low light (5 min) and high light (1 min) were recorded by using a PAM system, and the values were used for calculating Y(II). Mean values and standard errors derived from 6 biological replicates. The statistical analyses were performed by using ANOVA and the Dunnett's test (*P < 0.05, in comparison to the wild type).

Author contributions

P.G. conceived the project; L.-Y. H., P.G. designed the research; L.-Y.H. performed most of the experiments; M.L. performed GC-MS measurements; L.-Y. H., P.G. analyzed the data; P.G. supervised the experiments; L.-Y.H., P.G. wrote the article.

Acknowledgements

We thank Anne Bierling (LMU Munich) for the help of generating the double knock out mutants. We are also grateful to all green house staff in LMU Munich for taking care of Arabidopsis plants.

Funding

This work was supported by the Deutsche Forschungsgemeinschaft (TRR 175, B02)

Material distribution statement

The author responsible for distribution of materials integral to the findings presented in this article in accordance with the policy described in the Instructions for Authors is: Peter Geigenberger (geigenberger@bio.lmu.de).

Conflict of interest statement

The authors declare that they have no competing interests with others.

References

1. Allahverdiyeva, Y.; Suorsa, M.; Tikkanen, M.; Aro, E.M. Photoprotection of photosystems in fluctuating light intensities. *J. Exp. Bot.* **2015**, *66*, 2427–2436, doi:10.1093/jxb/eru463.
2. Armbruster, U.; Carrillo, L.R.; Venema, K.; Pavlovic, L.; Schmidtmann, E.; Kornfeld, A.; Jahns, P.; Berry, J.A.; Kramer, D.M.; Jonikas, M.C. Ion antiport accelerates photosynthetic acclimation in fluctuating light environments. *Nat. Commun.* **2014**, *5*, 5439, doi:10.1038/ncomms6439.
3. Foyer, C.H.; Noctor, G. Ascorbate and glutathione: The heart of the redox hub. *Plant Physiol.* **2011**, *155*, 2–18, doi:10.1104/pp.110.167569.
4. Geigenberger, P.; Fernie, A.R. Metabolic control of redox and redox control of metabolism in plants. *Antioxid. Redox Signal.* **2014**, *21*, 1389–421, doi:10.1089/ars.2014.6018.
5. Hasanuzzaman, M.; Borhannuddin Bhuyan, M.H.M.; Anee, T.I.; Parvin, K.; Nahar, K.; Al Mahmud, J.; Fujita, M. Regulation of ascorbate-glutathione pathway in mitigating oxidative damage in plants under abiotic stress. *Antioxidants* **2019**, *8*, 384, doi:10.3390/antiox8090384.
6. Noctor, G.; Mhamdi, A.; Chaouch, S.; Han, Y.; Neukermans, J.; Marquez-Garcia, B.; Queval, G.; Foyer, C.H. Glutathione in plants: An integrated overview. *Plant, Cell Environ.* **2012**, *35*, 454–484, doi:10.1111/j.1365-3040.2011.02400.x.
7. Smirnoff, N.; Wheeler, G.L. Ascorbic acid in plants: Biosynthesis and function. *Crit. Rev. Biochem. Mol. Biol.* **2000**, *35*, 291–314, doi:10.1080/10409230008984166.
8. Anjum, N.A.; Umar, S.; Chan, M.T. *Ascorbate-Glutathione Pathway and Stress Tolerance in Plants*; Anjum, N.A., Chan, M.-T., Umar, S., Eds.; Springer Netherlands: Dordrecht, 2010; ISBN 978-90-481-9403-2.
9. Reichheld, J.-P.; Khafif, M.; Riondet, C.; Droux, M.; Bonnard, G.; Meyer, Y. Inactivation of thioredoxin reductases reveals a complex interplay between thioredoxin and glutathione pathways in Arabidopsis development. *Plant Cell* **2007**, *19*, 1851–1865, doi:10.1105/tpc.107.050849.
10. Michelet, L.; Zaffagnini, M.; Marchand, C.; Collin, V.; Decottignies, P.; Tsan, P.; Lancelin, J.M.; Trost, P.; Miginiac-Maslow, M.; Noctor, G.; et al. Glutathionylation of chloroplast thioredoxin f is a redox signaling mechanism in plants. *Proc. Natl. Acad. Sci. U. S. A.* **2005**, *102*, 16478–16483,

doi:10.1073/pnas.0507498102.

11. Zaffagnini, M.; Michelet, L.; Marchand, C.; Sparla, F.; Decottignies, P.; Le Maréchal, P.; Miginiac-Maslow, M.; Noctor, G.; Trost, P.; Lemaire, S.D. The thioredoxin-independent isoform of chloroplastic glyceraldehyde-3- phosphate dehydrogenase is selectively regulated by glutathionylation. *FEBS J.* **2007**, *274*, 212–226, doi:10.1111/j.1742-4658.2006.05577.x.
12. Bashandy, T.; Guilleminot, J.; Vernoux, T.; Caparros-Ruiz, D.; Ljung, K.; Meyer, Y.; Reichheld, J.P. Interplay between the NADP-linked thioredoxin and glutathione systems in Arabidopsis auxin signaling. *Plant Cell* **2010**, *22*, 376–391, doi:10.1105/tpc.109.071225.
13. Gelhaye, E.; Navrot, N.; Macdonald, I.K.; Rouhier, N.; Raven, E.L.; Jacquot, J.P. Ascorbate peroxidase-thioredoxin interaction. *Photosynth. Res.* **2006**, *89*, 193–200, doi:10.1007/s11120-006-9100-x.
14. Vanacker, H.; Guichard, M.; Bohrer, A.-S.; Issakidis-Bourguet, E. Redox Regulation of Monodehydroascorbate Reductase by Thioredoxin y in Plastids Revealed in the Context of Water Stress. *Antioxidants* **2018**, *7*, 183, doi:10.3390/antiox7120183.
15. Meyer, Y.; Reichheld, J.P.; Vignols, F. Thioredoxins in Arabidopsis and other plants. *Photosynth. Res.* **2005**, *86*, 419–433, doi:10.1007/s11120-005-5220-y.
16. Meyer, Y.; Siala, W.; Bashandy, T.; Riondet, C.; Vignols, F.; Reichheld, J.P. Glutaredoxins and thioredoxins in plants. *Biochim. Biophys. Acta - Mol. Cell Res.* **2008**, *1783*, 589–600, doi:10.1016/j.bbamcr.2007.10.017.
17. Thormählen, I.; Ruber, J.; Von Roepenack-Lahaye, E.; Ehrlich, S.M.; Massot, V.; Hümmer, C.; Tezycka, J.; Issakidis-Bourguet, E.; Geigenberger, P. Inactivation of thioredoxin f1 leads to decreased light activation of ADP-glucose pyrophosphorylase and altered diurnal starch turnover in leaves of Arabidopsis plants. *Plant, Cell Environ.* **2013**, *36*, 16–29, doi:10.1111/j.1365-3040.2012.02549.x.
18. Yoshida, K.; Hara, S.; Hisabori, T. Thioredoxin selectivity for thiol-based redox regulation of target Proteins in Chloroplasts. *J. Biol. Chem.* **2015**, *290*, 14278–14288, doi:10.1074/jbc.M115.647545.
19. Thormählen, I.; Zupok, A.; Rescher, J.; Leger, J.; Weissenberger, S.; Groysman, J.; Orwat, A.; Chatel-Innocenti, G.; Issakidis-Bourguet, E.; Armbruster, U.; et al. Thioredoxins Play a Crucial Role in Dynamic Acclimation of Photosynthesis in Fluctuating Light. *Mol. Plant* **2017**, *10*, 168–

182, doi:10.1016/j.molp.2016.11.012.

20. Okegawa, Y.; Motohashi, K. Chloroplastic thioredoxin m functions as a major regulator of Calvin cycle enzymes during photosynthesis in vivo. *Plant J.* **2015**, *84*, 900–913, doi:10.1111/tpj.13049.
21. Benitez-Alfonso, Y.; Cilia, M.; San Roman, A.; Thomas, C.; Maule, A.; Hearn, S.; Jackson, D. Control of Arabidopsis meristem development by thioredoxin-dependent regulation of intercellular transport. *Proc. Natl. Acad. Sci. U. S. A.* **2009**, *106*, 3615–3620, doi:10.1073/pnas.0808717106.
22. Courteille, A.; Vesa, S.; Sanz-Barrio, R.; Cazalé, A.C.; Becuwe-Linka, N.; Farran, I.; Havaux, M.; Rey, P.; Rumeau, D. Thioredoxin m4 controls photosynthetic alternative electron pathways in Arabidopsis. *Plant Physiol.* **2013**, *161*, 508–520, doi:10.1104/pp.112.207019.
23. Collin, V.; Lamkemeyer, P.; Miginiac-Maslow, M.; Hirasawa, M.; Knaff, D.B.; Dietz, K.J.; Issakidis-Bourguet, E. Characterization of plastidial thioredoxins from arabidopsis belonging to the new y-type. *Plant Physiol.* **2004**, *136*, 4088–4095, doi:10.1104/pp.104.052233.
24. Lamkemeyer, P.; Laxa, M.; Collin, V.; Li, W.; Finkemeier, I.; Schöttler, M.A.; Holtkamp, V.; Tognetti, V.B.; Issakidis-Bourguet, E.; Kandlbinder, A.; et al. Peroxiredoxin Q of Arabidopsis thaliana is attached to the thylakoids and functions in context of photosynthesis. *Plant J.* **2006**, *45*, 968–981, doi:10.1111/j.1365-313X.2006.02665.x.
25. Navrot, N.; Collin, V.; Gualberto, J.; Gelhaye, E.; Hirasawa, M.; Rey, P.; Knaff, D.B.; Issakidis, E.; Jacquot, J.P.; Rouhier, N. Plant glutathione peroxidases are functional peroxiredoxins distributed in several subcellular compartments and regulated during biotic and abiotic stresses. *Plant Physiol.* **2006**, *142*, 1364–1379, doi:10.1104/pp.106.089458.
26. Bohrer, A.S.; Massot, V.; Innocenti, G.; Reichheld, J.P.; Issakidis-Bourguet, E.; Vanacker, H. New insights into the reduction systems of plastidial thioredoxins point out the unique properties of thioredoxin z from Arabidopsis. *J. Exp. Bot.* **2012**, *63*, 6315–6323, doi:10.1093/jxb/ers283.
27. Arsova, B.; Hoja, U.; Wimmelbacher, M.; Greiner, E.; Ustün, S.; Melzer, M.; Petersen, K.; Lein, W.; Börnke, F. Plastidial thioredoxin z interacts with two fructokinase-like proteins in a thiol-dependent manner: evidence for an essential role in chloroplast development in Arabidopsis and Nicotiana benthamiana. *Plant Cell* **2010**, *22*, 1498–515, doi:10.1105/tpc.109.071001.

28. Laloi, C.; Rayapuram, N.; Chartier, Y.; Grienenberger, J.M.; Bonnard, G.; Meyer, Y. Identification and characterization of a mitochondrial thioredoxin system in plants. *Proc. Natl. Acad. Sci. U. S. A.* **2001**, *98*, 14144–14149, doi:10.1073/pnas.241340898.
29. Martí, M.C.; Olmos, E.; Calvete, J.J.; Díaz, I.; Barranco-Medina, S.; Whelan, J.; Lázaro, J.J.; Sevilla, F.; Jiménez, A. Mitochondrial and Nuclear Localization of a Novel Pea Thioredoxin: Identification of Its Mitochondrial Target Proteins1[W]. *Plant Physiol.* **2009**, *150*, 646–657, doi:10.1104/pp.109.138073.
30. Ortiz-Espín, A.; Iglesias-Fernández, R.; Calderón, A.; Carbonero, P.; Sevilla, F.; Jiménez, A. Mitochondrial AtTrxo1 is transcriptionally regulated by AtbZIP9 and AtAZF2 and affects seed germination under saline conditions. *J. Exp. Bot.* **2017**, *68*, 1025–1038, doi:10.1093/jxb/erx012.
31. Calderón, A.; Sánchez-Guerrero, A.; Ortiz-Espín, A.; Martínez-Alcalá, I.; Camejo, D.; Jiménez, A.; Sevilla, F. Lack of mitochondrial thioredoxin o1 is compensated by antioxidant components under salinity in Arabidopsis thaliana plants. *Physiol. Plant.* **2018**, *164*, 251–267, doi:10.1111/ppl.12708.
32. Calderón, A.; Ortiz-Espín, A.; Iglesias-Fernández, R.; Carbonero, P.; Pallardó, F.V.; Sevilla, F.; Jiménez, A. Thioredoxin (Trx o1) interacts with proliferating cell nuclear antigen (PCNA) and its overexpression affects the growth of tobacco cell culture. *Redox Biol.* **2017**, *11*, 688–700, doi:10.1016/j.redox.2017.01.018.
33. Daloso, D.M.; Müller, K.; Obata, T.; Florian, A.; Tohge, T.; Bottcher, A.; Riondet, C.; Bariat, L.; Carrari, F.; Nunes-Nesi, A.; et al. Thioredoxin , a master regulator of the tricarboxylic acid cycle in plant mitochondria. *Proc. Natl. Acad. Sci. U. S. A.* **2015**, *112*, 1392–1400, doi:10.1073/pnas.1424840112.
34. Florez-Sarasa, I.; Obata, T.; Del-Saz, N.F.; Reichheld, J.-P.; Meyer, E.H.; Rodriguez-Concepcion, M.; Ribas-Carbo, M.; Fernie, A.R. The lack of mitochondrial thioredoxin TRXo1 affects in vivo alternative oxidase activity and carbon metabolism under different light conditions. *Plant Cell Physiol.* **2019**, *1*, 2369–2381.
35. Schwarzländer, M.; Fuchs, P. Keeping Mitochondrial Alternative Oxidase Reduced and Active in vivo Does Not Require Thioredoxin o1. *Plant Cell Physiol.* **2019**, *1*, 2357–2359, doi:10.1093/pcp/pcz123.
36. Reinholdt, O.; Schwab, S.; Zhang, Y.; Reichheld, J.-P.; Fernie, A.R.; Hagemann, M.; Timm, S. Redox-Regulation of Photorespiration through

Mitochondrial Thioredoxin o1. *Plant Physiol.* **2019**, *181*, 442–457, doi:10.1104/pp.19.00559.

37. Meng, L.; Wong, J.H.; Feldman, L.J.; Lemaux, P.G.; Buchanan, B.B. A membrane-associated thioredoxin required for plant growth moves from cell to cell, suggestive of a role in intercellular communication. *Proc. Natl. Acad. Sci. U. S. A.* **2010**, *107*, 3900–3905, doi:10.1073/pnas.0913759107.
38. Traverso, J.A.; Micalella, C.; Martinez, A.; Brown, S.C.; Satiat-Jeunemaître, B.; Meinnel, T.; Giglione, C. Roles of N-Terminal Fatty Acid Acylations in Membrane Compartment Partitioning: Arabidopsis h-Type Thioredoxins as a Case Study. *Plant Cell* **2013**, *25*, 1056–1077, doi:10.1105/tpc.112.106849.
39. Meyer, Y.; Vignols, F.; Reichheld, J.P. Classification of Plant Thioredoxins by Sequence Similarity and Intron Position. In *Methods Enzymol*; 2002; Vol. 347, pp. 394–402.
40. Marx, C.; Wong, J.H.; Buchanan, B.B. Thioredoxin and germinating barley: Targets and protein redox changes. *Planta* **2003**, *216*, 454–460, doi:10.1007/s00425-002-0857-7.
41. Serrato, A.J.; Cejudo, F.J. Type-h thioredoxins accumulate in the nucleus of developing wheat seed tissues suffering oxidative stress. *Planta* **2003**, *217*, 392–399, doi:10.1007/s00425-003-1009-4.
42. Park, S.K.; Jung, Y.J.; Lee, J.R.; Lee, Y.M.; Jang, H.H.; Lee, S.S.; Park, J.H.; Kim, S.Y.; Moon, J.C.; Lee, S.Y.; et al. Heat-shock and redox-dependent functional switching of an h-type Arabidopsis thioredoxin from a disulfide reductase to a molecular chaperone. *Plant Physiol.* **2009**, *150*, 552–561, doi:10.1104/pp.109.135426.
43. Laloi, C.; Mestres-Ortega, D.; Marco, Y.; Meyer, Y.; Reichheld, J.P. The Arabidopsis cytosolic thioredoxin h5 gene induction by oxidative stress and its W-box-mediated response to pathogen elicitor. *Plant Physiol.* **2004**, *134*, 1006–1016, doi:10.1104/pp.103.035782.
44. Reichheld, J.P.; Mestres-Ortega, D.; Laloi, C.; Meyer, Y. The multigenic family of thioredoxin h in Arabidopsis thaliana: Specific expression and stress response. *Plant Physiol. Biochem.* **2002**, *40*, 685–690, doi:10.1016/S0981-9428(02)01406-7.
45. da Fonseca-Pereira, P.; Souza, P.V.L.; Hou, L.-Y.; Schwab, S.; Geigenberger, P.; Nunes-Nesi, A.; Timm, S.; Fernie, A.R.; Thormählen, I.; Araújo, W.L.; et al. Thioredoxin h2 contributes to the redox regulation of mitochondrial

photorespiratory metabolism. *Plant Cell Environ.* **2020**, *43*, 188–208, doi:10.1111/pce.13640.

46. Hashida, S.N.; Kawai-Yamada, M. Inter-Organelle NAD Metabolism Underpinning Light Responsive NADP Dynamics in Plants. *Front. Plant Sci.* **2019**, *10*, doi:10.3389/fpls.2019.00960.
47. Gelhaye, E.; Rouhier, N.; Gérard, J.; Jolivet, Y.; Gualberto, J.; Navrot, N.; Ohlsson, P.-I.; Wingsle, G.; Hirasawa, M.; Knaff, D.B.; et al. A specific form of thioredoxin h occurs in plant mitochondria and regulates the alternative oxidase. *Proc. Natl. Acad. Sci. U. S. A.* **2004**, *101*, 14545–50, doi:10.1073/pnas.0405282101.
48. Jiménez, A.; Hernández, J.A.; Del Río, L.A.; Sevilla, F. Evidence for the presence of the ascorbate-glutathione cycle in mitochondria and peroxisomes of pea leaves. *Plant Physiol.* **1997**, *114*, 275–284, doi:10.1104/pp.114.1.275.
49. Marchand, C.; Le Maréchal, P.; Meyer, Y.; Miginiac-Maslow, M.; Issakidis-Bourguet, E.; Decottignies, P. New targets of Arabidopsis thioredoxins revealed by proteomic analysis. *Proteomics* **2004**, *4*, 2696–2706, doi:10.1002/pmic.200400805.
50. Yamazaki, D.; Motohashi, K.; Kasama, T.; Hara, Y.; Hisabori, T. Target Proteins of the Cytosolic Thioredoxins in Arabidopsis thaliana. *Plant Cell Physiol.* **2004**, *45*, 18–27, doi:10.1093/pcp/pch019.
51. Wong, J.H.; Balmer, Y.; Cai, N.; Tanaka, C.K.; Vensel, W.H.; Hurkman, W.J.; Buchanan, B.B. Unraveling thioredoxin-linked metabolic processes of cereal starchy endosperm using proteomics. *FEBS Lett.* **2003**, *547*, 151–156, doi:10.1016/S0014-5793(03)00696-3.
52. Balmer, Y.; Vensel, W.H.; Tanaka, C.K.; Hurkman, W.J.; Gelhaye, E.; Rouhier, N.; Jacquot, J.-P.; Manieri, W.; Schurmann, P.; Droux, M.; et al. Thioredoxin links redox to the regulation of fundamental processes of plant mitochondria. *Proc. Natl. Acad. Sci.* **2004**, *101*, 2642–2647, doi:10.1073/pnas.0308583101.
53. Fait, A.; Fromm, H.; Walter, D.; Galili, G.; Fernie, A.R. Highway or byway: the metabolic role of the GABA shunt in plants. *Trends Plant Sci.* **2008**, *13*, 14–19, doi:10.1016/j.tplants.2007.10.005.
54. Shelp, B.J.; Bozzo, G.G.; Trobacher, C.P.; Zarei, A.; Deyman, K.L.; Brikis, C.J. Hypothesis/review: Contribution of putrescine to 4-aminobutyrate (GABA) production in response to abiotic stress. *Plant Sci.* **2012**, *193–194*, 130–135, doi:10.1016/j.plantsci.2012.06.001.

55. Michaeli, S.; Fromm, H. Closing the loop on the GABA shunt in plants: Are GABA metabolism and signaling entwined? *Front. Plant Sci.* **2015**, *6*, 1–7, doi:10.3389/fpls.2015.00419.
56. Slocum, R.D. Genes, enzymes and regulation of arginine biosynthesis in plants. *Plant Physiol. Biochem.* **2005**, *43*, 729–745, doi:10.1016/j.plaphy.2005.06.007.
57. Facchini, P.J. Alkaloid biosynthesis in plants: Biochemistry, cell biology, molecular regulation, and metabolic engineering applications. Annual Review of Plant Physiology and Plant Molecular Biology 52:29-66. *Annu. Rev. Plant Physiol. Plant Mol. Biol* **2001**, *52*, 29–66.
58. Slocum, R.D.; Kaur-Sawhney, R.; Galston, A.W. The physiology and biochemistry of polyamines in plants. *Arch. Biochem. Biophys.* **1984**, *235*, 283–303, doi:10.1016/0003-9861(84)90201-7.
59. Li, T.; Xiao, Z.; Li, H.; Liu, C.; Shen, W.; Gao, C. A Combinatorial Reporter Set to Visualize the Membrane Contact Sites Between Endoplasmic Reticulum and Other Organelles in Plant Cell. *Front. Plant Sci.* **2020**, *11*, 1–15, doi:10.3389/fpls.2020.01280.
60. Hoffmann, C.; Plocharski, B.; Haferkamp, I.; Leroch, M.; Ewald, R.; Bauwe, H.; Riemer, J.; Herrmann, J.M.; Ekkehard Neuhaus, H. From endoplasmic reticulum to mitochondria: Absence of the arabidopsis ATP antiporter endoplasmic reticulum adenylate transporter1 perturbs photorespiration. *Plant Cell* **2013**, *25*, 2647–2660, doi:10.1105/tpc.113.113605.
61. Morales, A.; Kaiser, E. Photosynthetic Acclimation to Fluctuating Irradiance in Plants. *Front. Plant Sci.* **2020**, *11*, 1–12, doi:10.3389/fpls.2020.00268.
62. Selinski, J.; Scheibe, R. Malate valves: old shuttles with new perspectives. *Plant Biol.* **2019**, *21*, 21–30, doi:10.1111/plb.12869.
63. Huang, W.; Zhang, S.-B.; Hu, H. Sun leaves up-regulate the photorespiratory pathway to maintain a high rate of CO2 assimilation in tobacco. *Front. Plant Sci.* **2014**, *5*, doi:10.3389/fpls.2014.00688.
64. Ye, Z.P.; Liu, Y.G.; Kang, H.J.; Duan, H.L.; Chen, X.M.; Zhou, S.X. Comparing two measures of leaf photorespiration rate across a wide range of light intensities. *J. Plant Physiol.* **2019**, *240*, 153002, doi:10.1016/j.jplph.2019.153002.
65. Niedermaier, S.; Schneider, T.; Bahl, M.O.; Matsubara, S.; Huesgen, P.F. Photoprotective Acclimation of the Arabidopsis thaliana Leaf Proteome to Fluctuating Light. *Front. Genet.* **2020**, *11*, 1–15,

doi:10.3389/fgene.2020.00154.

66. Timm, S.; Florian, A.; Arrivault, S.; Stitt, M.; Fernie, A.R.; Bauwe, H. Glycine decarboxylase controls photosynthesis and plant growth. *FEBS Lett.* **2012**, *586*, 3692–3697, doi:10.1016/j.febslet.2012.08.027.
67. Timm, S.; Wittmiß, M.; Gamlien, S.; Ewald, R.; Florian, A.; Frank, M.; Wirtz, M.; Hell, R.; Fernie, A.R.; Bauwe, H. Mitochondrial dihydrolipoyl dehydrogenase activity shapes photosynthesis and photorespiration of Arabidopsis Thaliana. *Plant Cell* **2015**, *27*, 1968–1984, doi:10.1105/tpc.15.00105.
68. LaMontagne, E.D.; Collins, C.A.; Peck, S.C.; Heese, A. Isolation of Microsomal Membrane Proteins from Arabidopsis thaliana. *Curr. Protoc. Plant Biol.* **2016**, *1*, 217–234, doi:10.1002/cppb.20020.
69. Sweetlove, L.J.; Taylor, N.L.; Leaver, C.J. Isolation of intact, functional mitochondria from the model plant Arabidopsis thaliana. *Methods Mol. Biol.* **2007**, *372*, 125–136, doi:10.1007/978-1-59745-365-3_9.
70. Laemmli, U.K. Cleavage of structural proteins during the assembly of the head of bacteriophage T4. *Nature* **1970**, *227*, 680–685, doi:10.1038/227680a0.
71. Winer, J.; Jung, C.K.S.; Shackel, I.; Williams, P.M. Development and validation of real-time quantitative reverse transcriptase-polymerase chain reaction for monitoring gene expression in cardiac myocytes in vitro. *Anal. Biochem.* **1999**, *270*, 41–49, doi:10.1006/abio.1999.4085.
72. Schmittgen, T.D.; Zakrajsek, B.A.; Mills, A.G.; Gorn, V.; Singer, M.J.; Reed, M.W. Quantitative reverse transcription-polymerase chain reaction to study mRNA decay: Comparison of endpoint and real-time methods. *Anal. Biochem.* **2000**, *285*, 194–204, doi:10.1006/abio.2000.4753.
73. Roessner, U.; Luedemann, A.; Brust, D.; Fiehn, O.; Linke, T.; Willmitzer, L.; Fernie, A.R. Metabolic Profiling Allows Comprehensive Phenotyping of Genetically or Environmentally Modified Plant Systems. *Plant Cell* **2001**, *13*, 11–29, doi:10.1105/tpc.13.1.11.
74. Lisec, J.; Schauer, N.; Kopka, J.; Willmitzer, L.; Fernie, A.R. Gas chromatography mass spectrometry-based metabolite profiling in plants. *Nat. Protoc.* **2006**, *1*, 387–396, doi:10.1038/nprot.2006.59.
75. Erban, A.; Schauer, N.; Fernie, A.R.; Kopka, J. Nonsupervised Construction and Application of Mass Spectral and Retention Time Index Libraries From Time-of-Flight Gas Chromatography-Mass Spectrometry Metabolite Profiles.

Metabolomics. Methods Mol. Biol. **2007**, *358*, 19–38, doi:10.1007/978-1-59745-244-1_2.

76. Hou, L.Y.; Ehrlich, M.; Thormählen, I.; Lehmann, M.; Krahnert, I.; Obata, T.; Cejudo, F.J.; Fernie, A.R.; Geigenberger, P. NTRC Plays a Crucial Role in Starch Metabolism, Redox Balance, and Tomato Fruit Growth. *Plant Physiol.* **2019**, *181*, 976–992, doi:10.1104/pp.19.00911.
77. Luedemann, A.; Strassburg, K.; Erban, A.; Kopka, J. TagFinder for the quantitative analysis of gas chromatography - Mass spectrometry (GC-MS)-based metabolite profiling experiments. *Bioinformatics* **2008**, *24*, 732–737, doi:10.1093/bioinformatics/btn023.
78. Queval, G.; Noctor, G. A plate reader method for the measurement of NAD, NADP, glutathione, and ascorbate in tissue extracts: Application to redox profiling during Arabidopsis rosette development. *Anal. Biochem.* **2007**, *363*, 58–69, doi:10.1016/j.ab.2007.01.005.
79. Lintala, M.; Schuck, N.; Thormählen, I.; Jungfer, A.; Weber, K.L.; Weber, A.P.M.; Geigenberger, P.; Soll, J.; Bölter, B.; Mulo, P. Arabidopsis tic62 trol mutant lacking thylakoid-bound ferredoxin-NADP+ Oxidoredutase shows distinct metabolic phenotype. *Mol. Plant* **2014**, *7*, 45–57, doi:10.1093/mp/sst129.

Preprints (www.preprints.org) | NOT PEER-REVIEWED | Posted: 2 March 2021 doi:10.20944/preprints202103.0107.v1

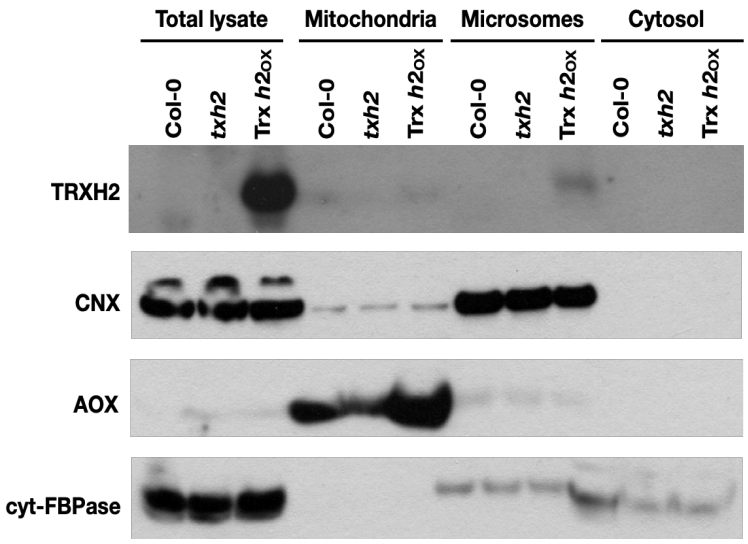

Figure 1. The enrichment of Trx *h*2 protein in different subcellular fractions. The wild-type plants (Col-0), knock out mutant (*trxh2*) and over expression line (Trx $h2_{ox}$) were grown under medium light condition for two weeks, and harvested for sample preparation. The detection of the TRXH2 protein and other subcellular protein markers was performed via immunoblot analysis. Calnexin (CNX) served as microsomal marker; cytosolic fructose-1,6-bisphosphatase (cyt-FBPase) served as cytosolic marker; alternative oxidase (AOX) served as mitochondrial marker.

Preprints (www.preprints.org) | NOT PEER-REVIEWED | Posted: 2 March 2021 doi:10.20944/preprints202103.0107.v1

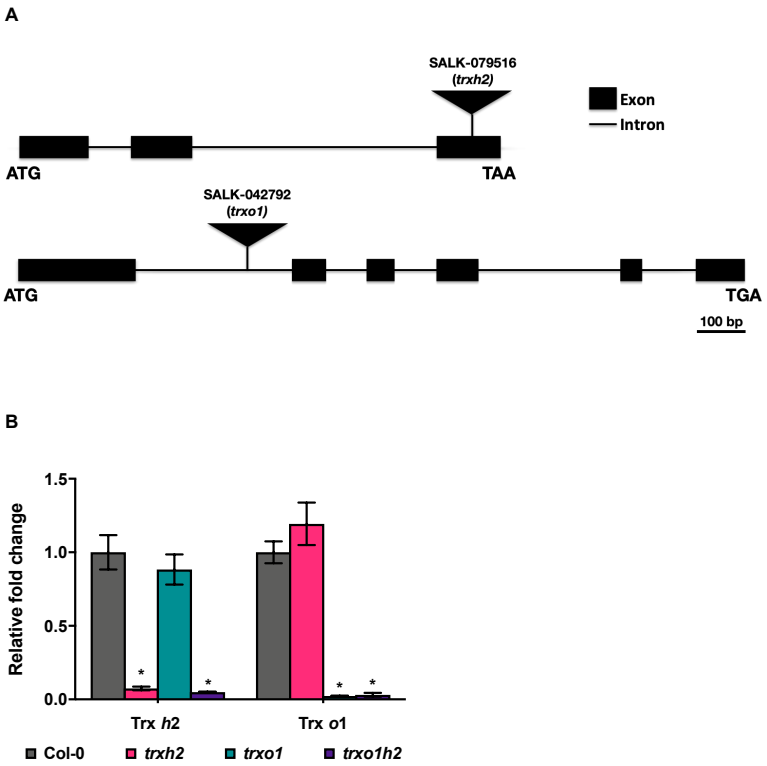

Figure 2. Molecular characterization of *trxh2*, *trxo1* and *trxo1h2*. A, The scheme of T-DNA insertion sites in *trxh2* and *trxo1* mutants. B, The transcript levels of Trx *h*2 and Trx *o*1 in mutant lines compared to the wild type (Col-0). Mean values and standard errors derived from 6 biological replicates. The statistical analyses were performed by using ANOVA and the Dunnett's test (*P < 0.05, in comparison to the wild type).

Preprints (www.preprints.org) | NOT PEER-REVIEWED | Posted: 2 March 2021 doi:10.20944/preprints202103.0107.v1

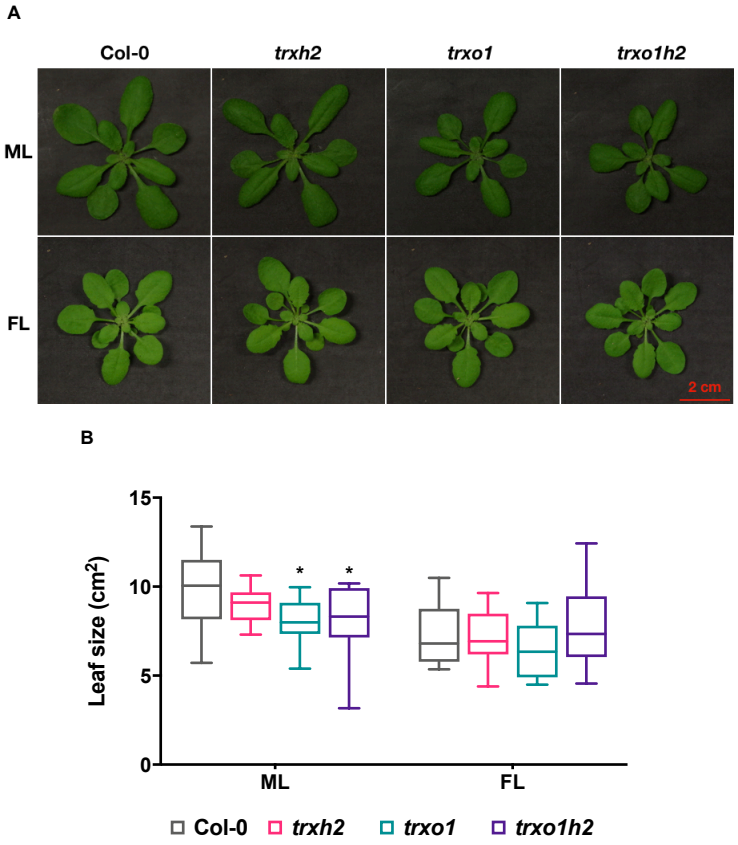

Figure 3. Growth phenotype of the wild type (Col-0) and mutant lines (*trxh2*, *trxo1* and *trxo1h2*) grown under medium (ML) or fluctuating (FL) light conditions. A, Visible phenotype of rosette leaves. B, The box plot of leaf size. Mean values derived from 10 to 14 plants. The statistical analyses were performed by using ANOVA and the Dunnett's test (*P < 0.05, in comparison to the wild type). Scale bar = 2 cm.

Preprints (www.preprints.org) | NOT PEER-REVIEWED | Posted: 2 March 2021 doi:10.20944/preprints202103.0107.v1

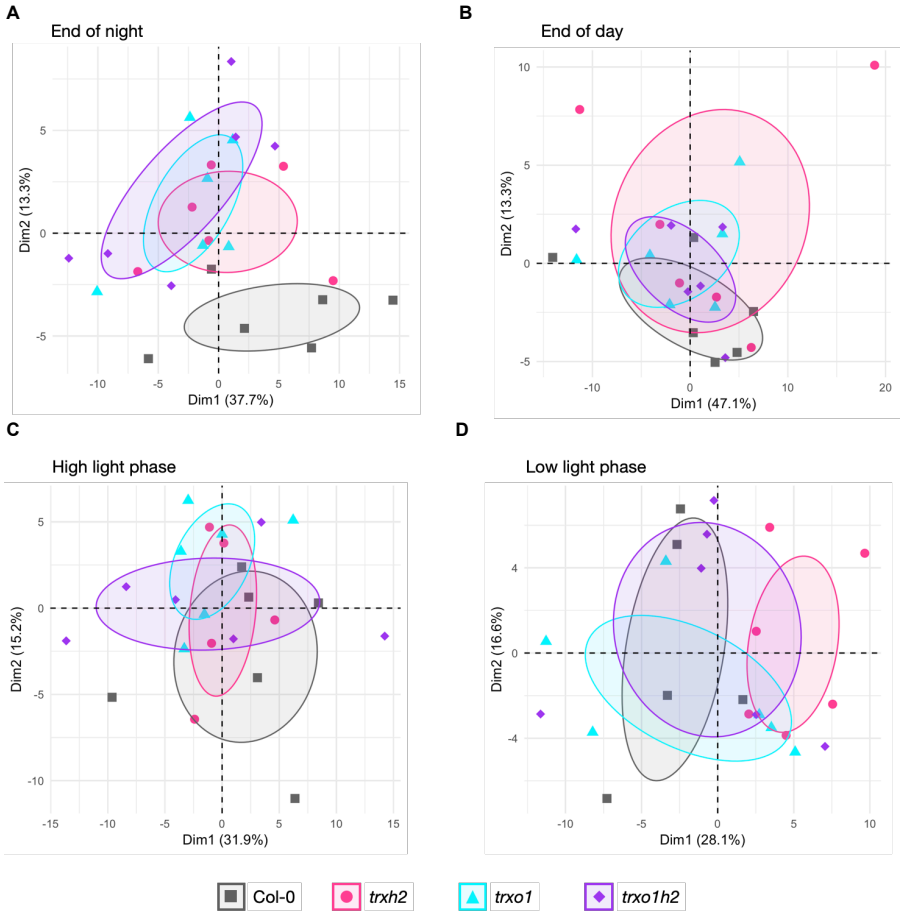

Figure 4. The principle component analysis on metabolite profile of the wild type (Col-0) and the mutant lines (*trxh2*, *trxo1* and *trxo1h2*). Arabidopsis plants grown under medium light condition were harvested at the end of night (A) and the end of day (B), respectively. Arabidopsis grown under fluctuating light condition were harvested at the high light phase (C) and low light phase (D), respectively. The samples were used for metabolite profiling via GC-TOF-MS, and the results were used for principle component analysis by using R software. Dim 1: 1st principle component; Dim 2: 2nd principle component.

Preprints (www.preprints.org) | NOT PEER-REVIEWED | Posted: 2 March 2021 doi:10.20944/preprints202103.0107.v1

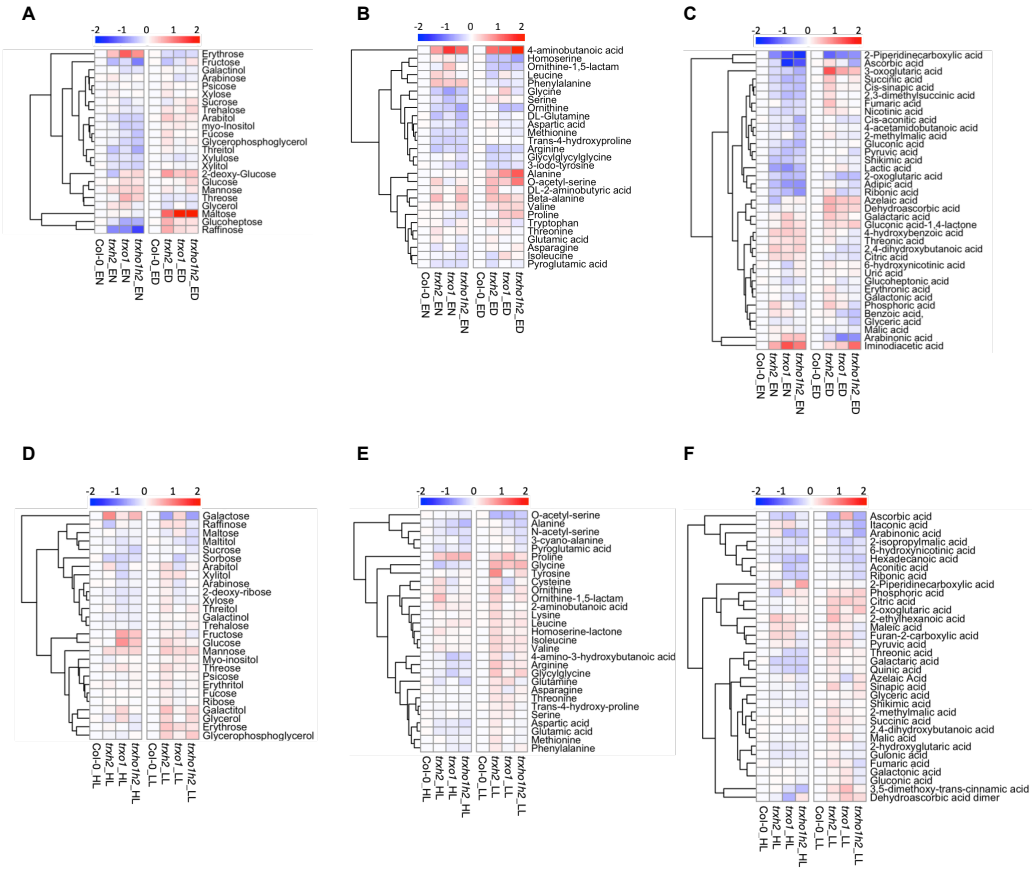

Figure 5. Metabolite profile of the wild type (Col-0) and the mutant lines (*trxh2*, *trxo1* and *trxo1h2*). Arabidopsis plants grown under medium light condition (A, B and C) were harvested at the end of night (EN) and the end of day (ED), respectively. Arabidopsis grown under fluctuating light condition (D, E and F) were harvested at the high light phase (HL) and low light phase (LL), respectively. The samples were used for metabolite profiling via GC-TOF-MS. A and D, Sugars and sugar alcohols. B and E, Amino acids. C and F, Organic acids and TCA cycle intermediates. Results are normalized to Col-0 with $\log_2$ transformation and visualized as a heatmap with hierarchical clustering done by R software. Data are taken from Table S1 and S2.

Preprints (www.preprints.org) | NOT PEER-REVIEWED | Posted: 2 March 2021 doi:10.20944/preprints202103.0107.v1

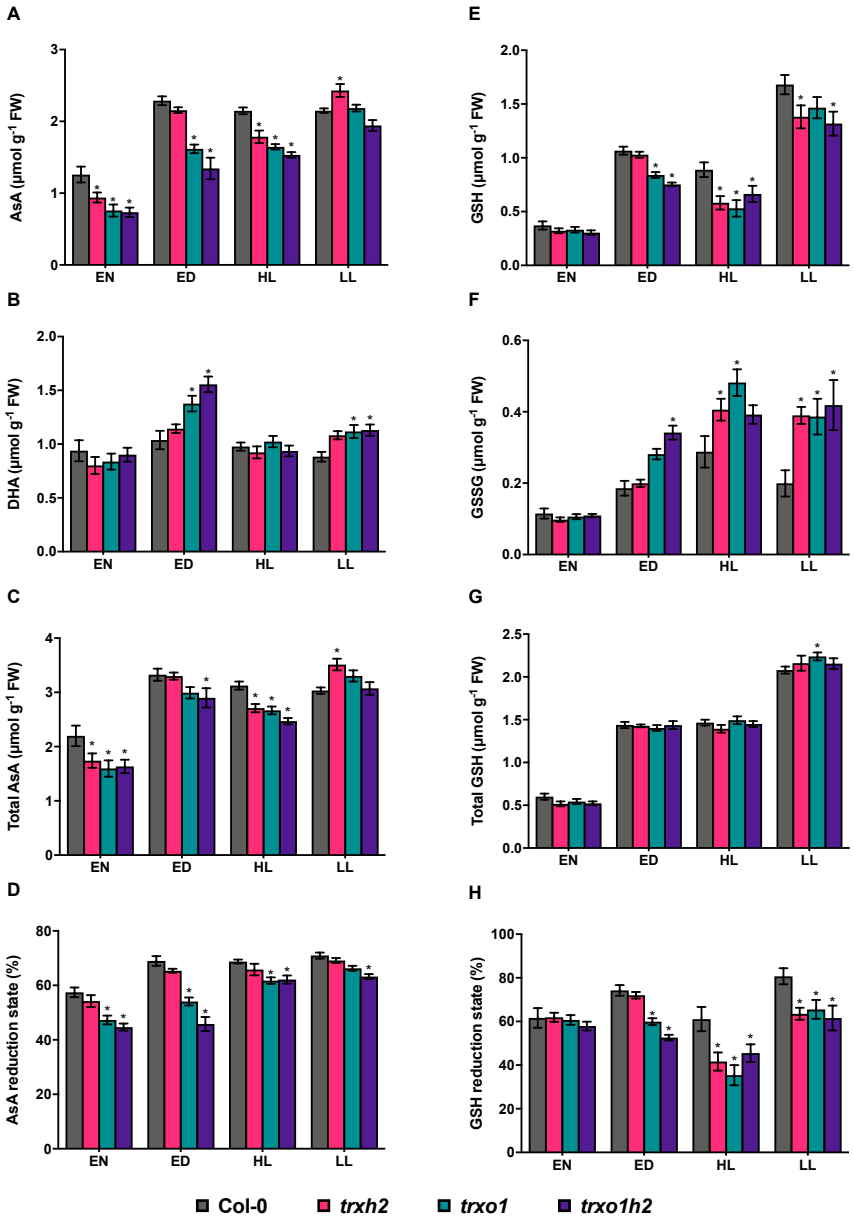

Figure 6. The redox couples of ascorbate (AsA) and glutathione (GSH) in the wild type (Col-0) and the mutant lines (*trxh2*, *trxo1* and *trxo1h2*). Arabidopsis plants grown under medium light condition were harvested at the end of night (EN) and the end of day (ED), respectively. Arabidopsis grown under fluctuating light condition were harvested at the high light phase (HL) and low light phase (LL), respectively. A, The level of ascorbate. B, The level of dehydroascorbate (DHA). C, The level of total AsA. D, The reduction state of AsA. E, The level of reduced GSH. F, The level of oxidized glutathione (GSSG). G, The level of total GSH. H, The reduction state of GSH. Mean values and standard errors derived from 6 biological replicates. The statistical analyses were performed by using ANOVA and the Dunnett's test (*P < 0.05, in comparison to the wild type).

Preprints (www.preprints.org) | NOT PEER-REVIEWED | Posted: 2 March 2021 doi:10.20944/preprints202103.0107.v1

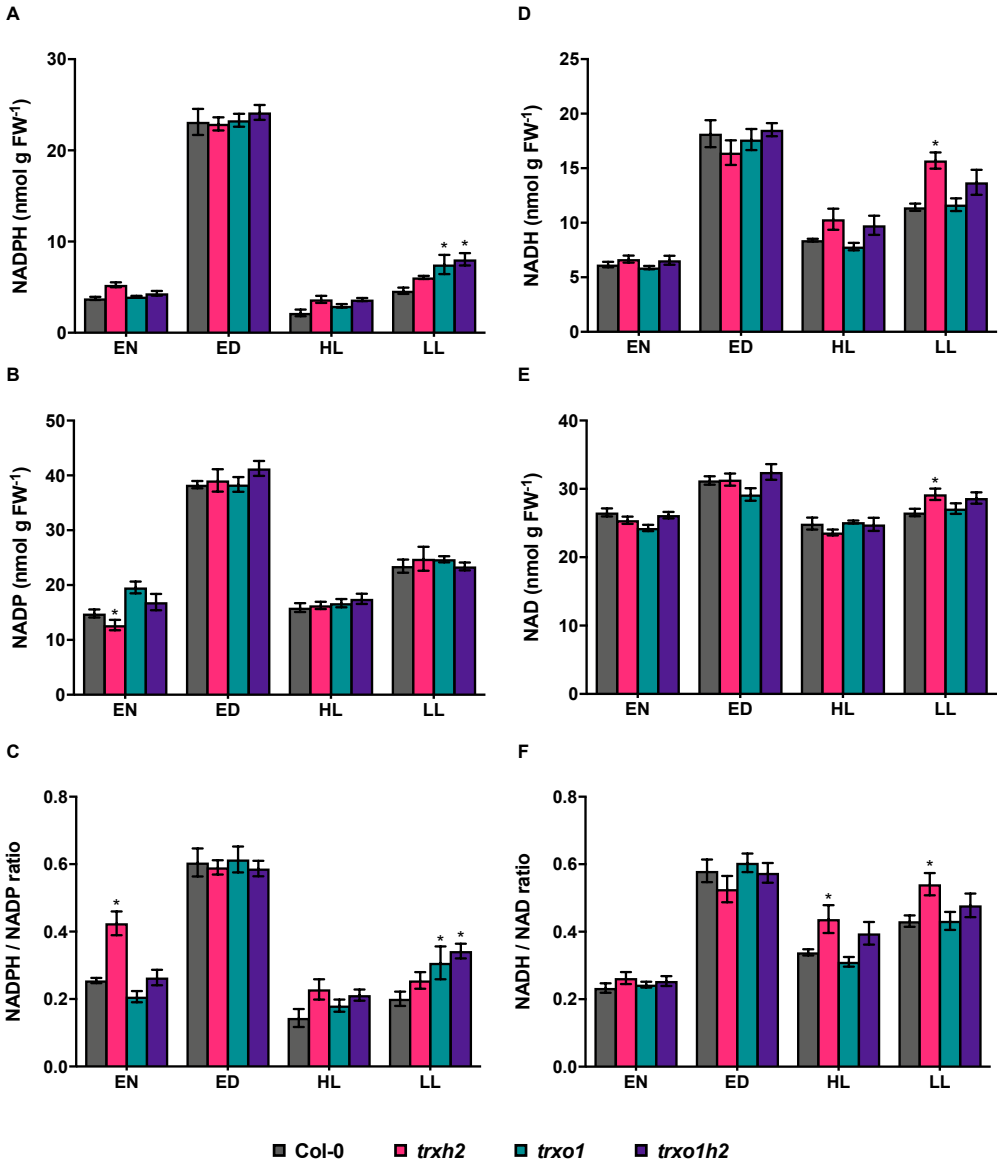

Figure 7. The redox couples of NADP(H) and NAD(H) in the wild type (Col-0) and the mutant lines (*trxh2*, *trxo1* and *trxo1h2*). Arabidopsis plants grown under medium light condition were harvested at the end of night (EN) and the end of day (ED), respectively. Arabidopsis grown under fluctuating light condition were harvested at the high light phase (HL) and low light phase (LL), respectively. A, The level of NADPH. B, The level of NADP. C, The NADPH-to-NADP ratio. D, The level of NADH. E, The level of NAD. F, The NADH-to-NAD ratio. Mean values and standard errors derived from 6 biological replicates. The statistical analyses were performed by using ANOVA and the Dunnett's test (*P < 0.05, in comparison to the wild type).

Preprints (www.preprints.org) | NOT PEER-REVIEWED | Posted: 2 March 2021 doi:10.20944/preprints202103.0107.v1

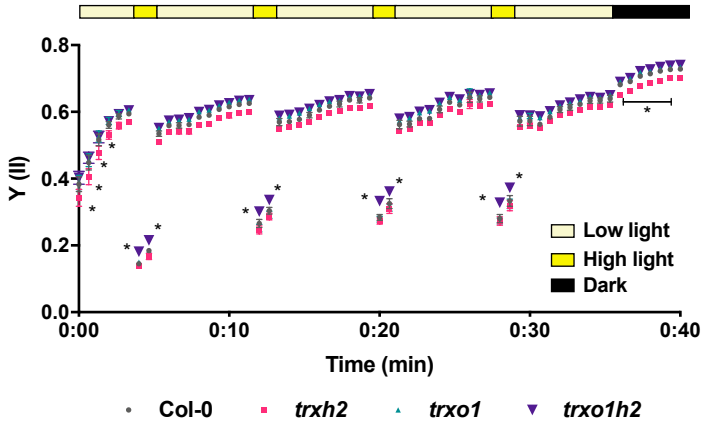

Figure 8. The quantum yield of photosystem II [Y(II)] in the wild type (Col-0) and the mutant lines (*trxh2*, *trxo1* and *trxo1h2*) in fluctuating light. Arabidopsis plants were grown in a fluctuating light environment for four weeks. Chlorophyll florescence kinetics during the alternating periods of low light (5 min) and high light (1 min) were recorded by using a PAM system, and the values were used for calculating Y(II). Mean values and standard errors derived from 6 biological replicates. The statistical analyses were performed by using ANOVA and the Dunnett's test (*P < 0.05, in comparison to the wild type).